2018

Streamwise Flow-Induced Oscillations of Bluff Bodies - The Influence of Symmetry Breaking

Tyler Gurian

STREAMWISE FLOW-INDUCED OSCILLATIONS OF BLUFF BODIES – THE INFLUENCE OF SYMMETRY BREAKING

A Thesis Presented

by

TYLER DOUGLAS GURIAN

Submitted to the Graduate School of the
University of Massachusetts Amherst in partial fulfillment
of the requirements for the degree of

MASTER OF SCIENCE IN MECHANICAL ENGINEERING

May 2018

Department of Mechanical and Industrial Engineering

STREAMWISE FLOW-INDUCED OSCILLATIONS OF BLUFF BODIES – THE INFLUENCE OF SYMMETRY BREAKING

A Thesis Presented

by

TYLER DOUGLAS GURIAN

Approved as to style and content by:

_____
Yahya Modarres-Sadeghi, Chair

_____
Jonathan Rothstein, Member

_____
David Schmidt, Member

_____
Sundar Krishnamurty, Department Head
Department of Mechanical and Industrial Engineering

ACKNOWLEDGEMENTS

Thanks to all members of the FSI Lab, especially Todd and Dan for their excellent experimental and technical knowledge. They have been a source of phenomenal knowledge and inspiration for me. Thanks to Professor Modarres for the confidence he has instilled in me, as well as his help in directing my focus.

To my family and friends, love you all.

ABSTRACT

STREAMWISE FLOW-INDUCED OSCILLATIONS OF BLUFF BODIES – THE INFLUENCE OF SYMMETRY BREAKING

MAY 2018

TYLER GURIAN, B.S., UNION COLLEGE (NY)

M.S.M.E. UNIVERSITY OF MASSACHUSETTS AMHERST

Directed by: Professor Yahya Modarres-Sadeghi

The influence of symmetry breaking on the flow induced oscillations of bluff bodies in the steamwise direction is studied. First, a series of experiments is conducted on a one-degree-of-freedom circular cylinder allowed to exhibit pure translational motion in the streamwise direction over a range of reduced velocities, $1.4 < U^* < 4.4$, corresponding to a Reynolds number range of $970 < Re < 3370$. These tests included displacement and force measurements and bubble flow visualizations. Two distinct regions of displacements were observed in reduced velocity ranges of $1.6 < U^* < 2.5$ and $2.75 < U^* < 3.85$. Measured force coefficients in the drag and lift direction were examined, along with the wake visualization, through the range of reduced velocities, to infer the resulting wake modes. Besides the symmetric, asymmetric and competitive shedding wake modes, which were observed previously, a new Alternating Symmetric (AS) mode was found, in which two vortices of opposite signs are shed per cycle of oscillations, but whose sizes relative to one another alternate for every cycle. This transition from symmetric to AS shedding occurred near the end of the first region of response. To investigate the influence of symmetry breaking, the circular cylinder was replaced with a square prism. Similar tests were run in the parameter space of $2.4 < U^* < 5.8$ and $757 < Re < 1900$ over angles of incidence of $0° \leq \alpha \leq 45°$. A distinct region of lock-in is observed for $\alpha = 0°$, 2.5°, 5°, 7.5° over $3.2 < U^* < 5.4$ for $\alpha = 0°$, and decreasing with increasing α. The wake structures were found to be roughly symmetric for $\alpha = 0°$, but transitioned towards asymmetry with increasing α. For $\alpha = 0°$ and 2.5° a gradual increase in the asymmetry of the fluid forcing was observed with increasing U^*, similar to that of the circular cylinder. In addition, wake structures of a perturbed square prism were observed for $\alpha = 20°$ and 30°. The vortex structures that formed were speculated to not project enough pressure in the direction of the degree of freedom to sustain oscillations.

TABLE OF CONTENTS

Page

LIST OF TABLES

Table Page

LIST OF FIGURES

Figure Page

CHAPTER 1

INTRODUCTION

Bluff bodies placed in flow shed vortices over a wide range of Reynolds numbers. This shedding results in time-varying forces on the structure and the frequency of the vortex shedding increases with flow velocity in accordance with the Strouhal Law. If the frequency of vortex shedding (and the resulting forcing frequency) intersects with the natural frequency of the structure, vortex-induced vibration (VIV) is observed. VIV is distinguished by relatively large-amplitude oscillations and vortex shedding that occur at the same frequency. VIV on a flexibly-mounted circular cylinder in the transverse (or crossflow) direction has been studied extensively (see Bearman 1984; Blevins 1990; Sarpkaya 2003; Williamson & Govardhan 2004; Vandiver 2012). Less work has been done on VIV in the streamwise or inline direction.

Early experiments by Aguirre (1977) and later by Okajima *et al.* (2002) showed that the response of the inline system is characterized by two distinct regions of non-zero amplitudes, the first occurring at a reduced velocity, U^* of approximately 1.7 ($U^* = U/f_{nw}D$, where U is the flow velocity, f_{nw} is the system's natural frequency in water, and D is the cylinder's diameter). It was noticed that this region of response occurred at a lower U^* than would initially be expected if the fluid excitation forces were due to asymmetric vortex shedding. With a Strouhal Number of $St = 0.2$ ($St = f_{St}D/U$, where f_{St} is the asymmetric vortex shedding frequency for a fixed circular cylinder) holding for a wide range of Reynolds numbers, streamwise excitation should occur at approximately $U^* = 2.5$, where the frequency of fluctuating forces due to asymmetric shedding approaches the structure's natural frequency. A second region of response was also observed at this point, with the two regions separated by a region of low-amplitude response. In addition, wake modes were classified and found to be distinct between the two regions. Symmetric shedding was found to dominate the first region of response, in which two vortices of opposite signs are shed at the same time (one from each side of the cylinder) in one cycle. Symmetric vortices have been recognized as the source of fluid forcing for this first region. (King 1977; King *et al.* 1973; Okajima *et al.* 2002). Asymmetric vortices dominate the second region of response (Okajima *et al.* 2002).

Okajima *et al.* (2002) tested two different experimental set-ups, a circular cylinder mounted as a cantilevered beam and a circular cylinder supported elastically at both ends (but whose displacement resulted in small yet inherent displacement in the crossflow direction as well) over a range of Reynolds numbers, $800 < Re < 4000$. The non-cantilevered cylinder was found to exhibit two distinct regions of excitation, one beginning at $U^* = 1.4$, and the second

beginning at $U^* = 2.5$, separated by a region of low-amplitude response. It was found that larger reduced mass-damping parameters, C_n ($C_n = 2m^*\delta$ and $m^* = m/\rho D^2$, where δ is the logarithmic decrement of the structure's damping parameter in otherwise still water, m is the mass per unit length of the cylinder, and ρ is the fluid density), reduce the amplitude of response significantly. The lowest value of mass-damping parameter in their experiment, $C_n = 0.77$, resulted in a maximum response amplitude of approximately 5% of the cylinder diameter for the non-cantilevered cylinder, compared to only 1.5% for $C_n = 1.64$. The cantilevered cylinder responded with a single, larger amplitude region, which also began at $U^* = 1.4$ with a maximum amplitude of ~9% of the cylinder's diameter. The magnitude of oscillations for the cantilevered cylinder was larger than the non-cantilevered set-up: 9% compared to 5%. However, the cantilevered cylinder had a lower reduced mass-damping parameter: $C_n = 0.24$ compared to $C_n = 0.77$.

Another experimental study using a flexibly-mounted cantilevered circular cylinder free to vibrate in the streamwise direction was carried out by Sherwood *et al.* (2009) over a Reynolds number range of $120 < Re < 2900$ in both steady and pulsating flow. The nature of the cantilevered beam set-up meant that displacements also resulted in a rotation of the free end, and small displacements in the crossflow direction. For pulsating flow with $Re = 920$ and $U^* = 2.75$ based on mean flow velocity, and for $f_e/f_{nw} = 1.15$ and $f_e/f_{St} = 1.9$ (where f_e is the flow pulsation frequency) amplitudes of oscillations were found to increase up to 400\% compared to the steady flow case (Sherwood *et al.* 2009). Phasing between the cylinder oscillations and flow pulsation was not discussed and could have contributed to the large increase in oscillation magnitude.

Cagney and Balabani (2013a) observed the response of a flexibly-mounted circular cylinder over a range of $450 < \mathrm{Re} < 3700$ free to translate in the in-line direction of flow. The experimental set-up allowed for a very limited but present rotational motion of the cylinder about an axis perpendicular to the flow, and the cylinder's tip motion due to this rotation found to be less than 5% of that due to translation (Cagney and Balabani 2013a). The cylinder's response was observed as a function of true reduced velocity, U^*St/f^* (where f^* is the ratio of the system's response frequency to the system's natural frequency, $f^* = f/f_{nw}$, where two distinct regions of response were found to exist similar to those of Okajima *et al.* (2002), but with smaller amplitudes in both regions. This discrepancy in amplitude can most likely be attributed to significant differences in the experimental set-ups between the two cases (Konstantinidis 2014) Particle Image Velocimetry (PIV) was used (Cagney and Balabani 2013a) to observe and quantify the wake over the entire response range. A symmetric (S-I) wake mode, in which only

one pair of vortices remain symmetric in the far wake, was observed for a true reduced velocity of $U^*St/f^* = 0.36$, corresponding to $U^* = 2.1$. The wake mode for other responses was found to be asymmetric. Using PIV, Cagney and Balabani (2013a) distinguished between the two different asymmetric wake modes deemed A-II and SA, which have been noted in other studies that have analyzed the wake using quantitative methods (Jauvtis and Williamson 2014); A-II vortex shedding is asymmetric vortex shedding characterized by two single vortices shed per cycle of oscillations, reminiscent of von Karman vortex shedding, while SA, or Streamwise-Asymmetric, vortex shedding is characterized by the same number of vortices as A-II shedding, but each vortex is shed along the centerline of the structure.

An experimental study by Cagney and Balabani (2014) compared the response of a 2-DOF pivoted cylinder with that of the 1-DOF cylinder from Cagney and Balabani (2013a) for $U^* < 4$. The response was found to be similar, with two branches of large-amplitude response separated by a region of low-amplitude response for reduced velocity range of $2.5 < U^* < 2.8$. The first branch of response within $1.7 < U^* < 2.5$ was found to be similar for both the 1-DOF and 2-DOF systems, with streamwise oscillations dominating the 2-DOF system and similar wake modes for both systems. For the second response region, $2.8 < U^* < 4$, the 2-DOF system exhibited less wake-mode competition than the 1-DOF system. In other words, the A-II mode was by far the dominant shedding mode, while the probability of observing symmetric shedding was negligible (Cagney and Balabani 2014).

Detailed studies into the wake of an inline system have been carried out. Al-Mdallal *et al.* (2007) performed a 2D computational study of forced circular cylinder streamwise oscillations at two oscillation amplitudes, $A^* = 0.1, 0.3$ ($A^* = A/D$ where A is the oscillation amplitude) and a frequency range of $0.5 < f_c/f_{St} < 3$ (where f_c is the cylinder's forcing frequency). A transition to symmetric shedding was found at $A^* = 0.3$ as the forcing frequency approached and surpassed $f_c/f_{St} = 2$. This is comparable with approaching a U^* of approximately 2.5 from larger values and decreasing to U^* of approximately 1.8, (U^* and f_c/f_{St} are inversely related). In their study, only asymmetric shedding was found for the lower amplitude, $A^* = 0.1$.

Konstantinidis and Balabani (2007), using PIV, studied the wake of a fixed circular cylinder subjected to streamwise flow perturbations of varying frequencies, $3 < f_e/f_{St} < 4$. This situation is analogous to a flexibly-mounted cylinder in an otherwise steady flow, and is roughly equivalent to observing reduced velocities of $1 < U^* < 2$. At lower frequency ratios (corresponding to the higher U^* values), various symmetric shedding modes were found to be dominant, while asymmetric modes became increasingly more dominant as the frequency exceeded $f_e/f_{St} = 3.8$. Furthermore, Konstantinidis and Balabani (2007) used these results to

show that fluctuating drag force is in phase with the relative cylinder displacement, and qualitatively consistent with the results of Nishihara *et al.* (2005), who experimentally studied the forces on a cylinder forced to oscillate in the streamwise direction.

In a separate study, Cagney and Balabani (2013b) investigated mode competition in the wake of a flexibly-mounted in-line circular cylinder for a single parameter set with a true reduced velocity of $U^*St/f^* = 0.42$, corresponding to $U^* = 2.2$. Using PIV and an identical experimental set-up, they found that the symmetric (S-I) shedding mode was less stable than the asymmetric (A-II) mode for this reduced velocity. In 3000 velocity fields that were analyzed, the S-I mode was found in only 8% compared to 92% for the A-II mode (Cagney and Balabani 2013b).

The second region of response was investigated in more details by Cagney and Balabani (2013c). PIV was used to examine the existence of multiple wake modes in the second region of response, and the effect of hysteresis on the amplitude response was investigated. They found that varying the reduced velocity from high to low in a decreasing fashion resulted in a narrower second region of response and an A-II shedding mode Cagney and Balabani (2013c). When the reduced velocity was varied from small to large in increasing fashion, both SA and A-IV modes were observed. It was observed that the SA mode resulted in larger amplitude oscillations than the A-IV mode, but that both were stable.

In a recent study by Ulveseter *et al.* (2017), a time domain model was created to model the response of a flexibly-mounted cylinder using parameters derived empirically from forced-oscillation studies. Results were compared with free response results from \cite{Johansen} and were found to be in fair agreement. Discrepancies in amplitude were attributed to the simplicity of the model (Ulveseter *et al.* 2017). These results also are in fair agreement with previous experimental results (Okajima et al. 2002; Cagney and Balabani 2013a).

A detailed numerical study by Bourguet and Jacono (2015) looked at the response of a circular cylinder with a degree of freedom in the streamwise direction and an imposed rotation about its axis at a Reynolds number of $Re = 100$. For the case of no rotation, a zero-amplitude response was calculated for the cylinder over all values of reduced velocity. This is consistent with experimental results (Okajima et al. 2002; Cagney and Balabani 2013a), as non-zero response has only been measured at Reynolds numbers one or more orders of magnitude larger. No response in the inline direction has been observed based on numerical results, due to the low *Re* used.

In general, FIV (flow-induced vibrations) of a flexibly-mounted square prism in the crossflow direction, as well as flow past a rigidly-mounted square prism, is thoroughly studied (see Bearman *et al.* 1987, Blevins 1990, Naudascher and Rockwell 1994, Nemes *et al*. 2012). In particular, Nemes *et al.* (2012) have presented a very thorough investigation, discussing the amplitude response, and wake modes of a square prism flexibly-mounted in the crossflow direction over angles of incidence of $0° < \alpha < 45°$, where angle of incidence, α, is defined as 0 when one side of the square cross section is directly perpendicular to the flow. The response ranged from VIV (similar to that of a circular cylinder) at $\alpha = 45°$, to a large-amplitude galloping response at $\alpha = 0°$. Nemes *et al*. (2012) also investigated the complex transition between the two phenomena as α was increased.

The square cross section is particularly interesting because it remains one of the simplest cross sections that is capable of exhibiting this galloping type response when mounted flexibly in the crossflow direction. Galloping can be described as high amplitude, velocity dependent, low frequency ($f^* < 1$) oscillatory response (Nemes *et al.* 2012). Galloping can occur for certain cross sections if structural displacement causes a relative flow velocity with respect to the structure, and this relative velocity creates a lift force in the same direction as displacement (Paidoussis *et al.* 2011). This feedback loop serves as negative damping which the structure feeds off to create larger amplitude oscillations as flow velocity is increased.

General characteristics of steady flow past a rigid square cylinder have also been investigated. Obasaju (1984) conducted a series of experiments in a wind tunnel on a rigidly mounted square cylinder with dimensions $D = 51$ mm (where D is the side length of the square) and $L = 900$ mm (approximately). A variety of measurements were taken, in particular the Strouhal number and coefficient of drag were measured as functions of angle of incidence α. It was found that coefficient of drag decreased sharply from a value of $C_D = 2.2$ to $C_D = 1.3$ over $0° < \alpha < 13.5°$, at which point it began increasing slowly again. The Strouhal number exhibited the opposite trend, increasing sharply from a value of $St = 0.125$ to $St = 0.175$ over $0° < \alpha < 13.5°$, but then slowly decreasing thereafter.

Knisley (1990) performed a set of experiments on the Strouhal numbers of rectangular cross sections. This included a square prism cross section (where the ratio of side lengths was equal to 1). The findings were very similar to that of Obasaju (1984), confirming the trend of a decreasing C_D and increasing St as angle of incidence varied over $0° < \alpha < 13.5°$, then slowly increasing and decreasing (respectively) after that point. The values reported by C. W. Knisley (1990) were very similar to that of Obasaju (1984).

Knisley (1990) also briefly discussed the effect that square prism edge quality might have on the Strouhal number. It was stated that rounded edges (as supposed to perfectly sharp ones) may have the tendency to increase *St*. The square prism used in the experiments presented here in this document was created using a 3D printer and possess the sharpest corners that the printer is capable of delivering.

A set of water tunnel experiments by Dutta *et al.* (2008) used PIV, hot wire anemometry, and flow visualization particles to investigate C_D and *St* values of a square prism at angles of incidence α = 0°, 22.5°, 30°, and 45°. Consistent with past studies a min and max C_D and *St* (respectively) were found at an angle of incidence of α = 22.5°.

The existence of a critical angle of incidence is clear. As discussed, experiments on a rigidly-mounted square prism have shown a sharp change in the behavior of C_D and *St* at an angle of incidence of approximately α = 13.5°. In addition, Rockwell (1977) discussed the flow field phenomena responsible for this critical angle. Namely, it is the reattachment of the separated boundary later to the face of the square cross section that was originally parallel to the flow at α = 0°.

The response of a square prism flexibly-mounted in the streamwise direction has received considerably less attention. In a comprehensive collection of FIV studies, Naudascher (1987) presented results of a rigid square prism with D = 60 mm and L = 683 mm, flexibly mounted in a wind tunnel with a degree of freedom in the streamwise direction. The angle of incidence was varied 0° < α < 45°. The square prism tested by Naudascher had a mass ratio m^* = 425. However, the system possessed very low structural damping, with damping ratio of ζ = .0028. For angles of incidence of 0° < α < 13.5°, a region of displacement response over a reduced velocity range of approximately 4 < U^* < 5 was found to approach 10% of the cylinders side length at α = 0°, with the amplitude in this region decreasing with increasing α. A region of smaller amplitude response was also observed in a reduced velocity range 7 < U^* < 8, with amplitudes increasing with increasing α. For 14.5° < α < 35°, the first region of response disappears, with the second region (7 < U^* < 8) becoming much more prevalent, approaching 10% of square's side length at α = 13.5°. The amplitude of this second region decreased from there with higher values of α. The frequency of all oscillations reported by Naudascher (1987) were very near that of the natural frequency of the system (f^* = 1). Wake modes for α = 0° and U^* = 4 were also observed. Symmetric (two vortices of opposite sign shed per cycle of oscillation) and asymmetric vortices were observed for these parameters.

The goal of the present work is to investigate and compare the response of two rigid bluff bodies, a circular cylinder, and a square prism, flexibly mounted with a degree of freedom

in the streamwise direction. The effect of passively breaking the symmetry of the system by imposing an angle of incidence on the square prism will be investigated. For the first time, forces will be measured for a streamwise system free to oscillate so that they can be observed in conjunction with flow visualization.

CHAPTER 2

CIRCULAR CYLINDER

2.1 Experimental Set Up

A circular cylinder with an outside diameter of D = 25.4 mm and a submerged length of L = 355.5 mm corresponding to an aspect ratio of 14 was tested in a recirculating water tunnel. The cylinder was made of hollow aluminum tubing with a wall thickness of 1.59 mm. This tubing was sealed to ensure that none of the surrounding fluid would find its way into the hollow section. This cylinder was mounted on an air bearing system that allowed pure, 1D, translational motion in the streamwise direction, and provided very low structural damping. The cylinder was mounted to these bearings through a 3D-printed adapter, a force sensor, and a mounting plate as seen in figure 1. The structural damping ratio was measured experimentally using a decay test and was found to be $\zeta = 0.006$. Springs were attached from the mount plate on the air bearings to a fixed mounting point. The mass ratio for the circular cylinder was $m^* = 1.61$. The moving mass accounted for the mass of every component that was moving with the cylinder, including the force sensor, air bearings, mount plate, and 3D-printed adapter.

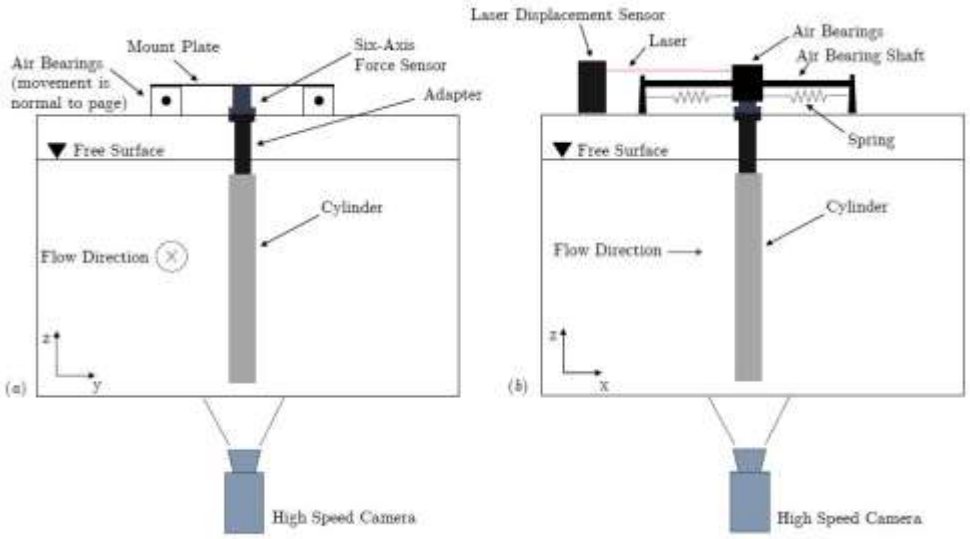

Figure 1: Schematic of the Inline VIV set-up when *(a)* looking in the direction of flow, with flow normal to the page, and *(b)* looking perpendicular to flow, with flow from left to right.

2.2 Flow Quality

A recirculating water tunnel with the test-section dimensions of 1.27 m x 0.5 m x 0.38 m was used for this series of experiments. To ensure uniform flow and accurate velocity, bubble

image velocimetry (BIV) was used to obtain flow profiles at varying test-section depths. The details of this procedure are documented in Seyed-Aghazadeh *et al.* (2017).

2.3 Data Collection

Data were collected for this experiment with two different sensors. Displacements were recorded using a Micro-Epsilon ILD 1402-600 non-contacting laser displacement sensor. This sensor was synchronized with an ATI-Nano17/IP68 six-axis force sensor. The force sensor was mounted between the cylinder and the mounting plate to ensure that all fluid forces were captured. The laser displacement sensor was aligned parallel to the direction of motion. The nature of the set-up was such that the force sensor captured the inertial forces of the structure as well as flow forces on the structure. The force data were post processed to remove the inertial component from the time series. Decay tests were recorded using these sensors to acquire system specifications. These tests were conducted by giving the system an initial displacement and allowing displacement data to be recorded for at least 15 cycles of oscillations. The system's natural frequency and damping ratio were calculated from this time history. The system's natural frequency in water was found to be $f_{nw} = 1.19$ Hz. The system's natural frequency in air was found to be $f_n = 1.51$ Hz.

The experiments were started at a flow velocity of 0.04 m/s and the flow velocity was increased in increments of 0.003 m/s up to 0.13 m/s. This corresponds to a Reynolds number range of $970 < Re < 3370$. Force and displacement data were collected for at least 90 seconds at each flow velocity. The data from the force sensor were collected in tandem with those of the displacement sensor so that the respective time histories were synchronized.

Hydrogen bubble generation was used for flow visualization. A detailed description of the system used for hydrogen bubble generation is documented in Seyed-Aghazadeh *et al.* (2017). Hydrogen bubbles were generated through the electrolysis of water. A platinum wire with a diameter of 0.0508 mm was strung across the test section perpendicular to the flow and the cylinder's long axis. The platinum wire served as an anode, while a positively charged graphite plate served as a cathode. The potential between the two caused a build-up of hydrogen bubbles on the platinum wire. The bubbles separated from the wire once their diameter exceeded the wire diameter, creating a bubble film. This film of bubbles was used to view the wake structure. The wake images were captured using a Phantom Miro M110 high speed camera.

2.4 The General Behavior of the Cylinder

The response of the system is characterized by two regions of relatively large-amplitude oscillations and one intermediate region with a very small amplitude of oscillations. The first non-zero amplitude region occurs in the reduced velocity range of $1.6 < U^* < 2.5$, and the second region occurs in a reduced velocity range of $2.75 < U^* < 3.85$. These results are plotted in figure 2a. The dimensionless amplitude of oscillations, A^* ($A^* = A/D$, where $A = \sqrt{2}(x_{rms})$, and x is the displacement signal), approaches 0.08 in the first region and 0.06 in the second region. The general behavior of these results is in agreement with previous experimental studies (Okajima *et al.* 2002; Johansen 2004; Cagney & Balabani 2013a) and also corresponds well with the time-domain model created by Ulveseter *et al*. (2017). Differences between this and previous studies come mostly in the form of relative amplitudes between the two regions of response. For example, Okajima *et al.* (2002) found a larger amplitude of response for the second region of response. This can be attributed to differences in experimental set-ups.

The dimensionless frequency is shown in figure 2b, in which $f^* = f/f_{nw}$, (where f is the frequency of oscillations). While the response frequency remains very close to $f^* = 1$, it increases slightly over the range of reduced velocities, due to the variation of added mass with reduced velocity as discussed by Cagney and Balabani (2013a) for inline VIV. This is also discussed for crossflow VIV by Williamson and Govardhan (2004).

A line corresponding to $2St$ is plotted in figure 2b. Rather counterintuitively, the point at which the drag forcing frequency intersects the system's natural frequency in still water corresponds to a dramatic decrease in the amplitude of the system response. However, this behavior is in agreement with studies which have established the existence of negative fluid excitation (or positive fluid damping) for oscillation frequencies at or slightly higher than $2St$ (Konstantinidis 2014).

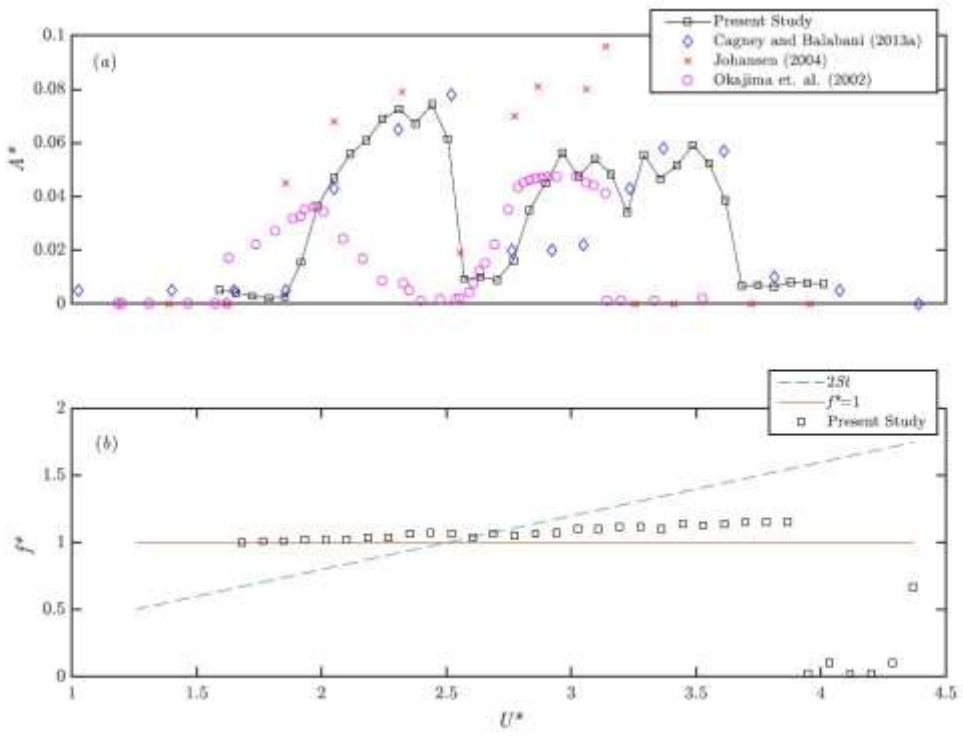

Figure 2: *(a)* Dimensionless displacement amplitude, *A**, versus reduced velocity, *U**, for the current study as well as previous studies, together with *(b)* the displacement frequency ratio, *f**, versus *U** for the present study.

The magnitude of fluctuating drag coefficient C_D ($C_D = 2F_D/U^2DL\rho$, where F_D is the fluctuating drag force) is plotted in figure 3a. Inertial forces associated with the acceleration of the cylinder were removed in the processing of the data, and do not contribute to the magnitude of the fluctuating drag coefficient. The magnitude of the fluctuating drag (or inline) force (figure 3a) is strongly correlated with the response of the system in the regions of non-zero amplitude. The largest values of fluctuating drag force occur in the range of reduced velocities corresponding to the first non-zero response region. The dominant frequency of fluctuating drag coefficient (figure 3b) coincides with f_{nw} and increases slightly with reduced velocity similar to the increase in oscillation frequency in the displacement response (figure 2b). Since the fluctuating drag force is inherently related to the frequency of vortex shedding, it can be said that lock-in is observed for the entire range of reduced velocities in which the cylinder exhibits a non-zero response. This characterization is consistent with the definition of lock-in in which there is synchronization between structure's oscillations and vortex shedding. The mean value of drag coefficient (figure 3c) fluctuates in different ranges of response. The horizontal line in figure 3c corresponds to the value of mean drag coefficient of a fixed cylinder for this range of Reynolds numbers found by Gopalkirshnan.

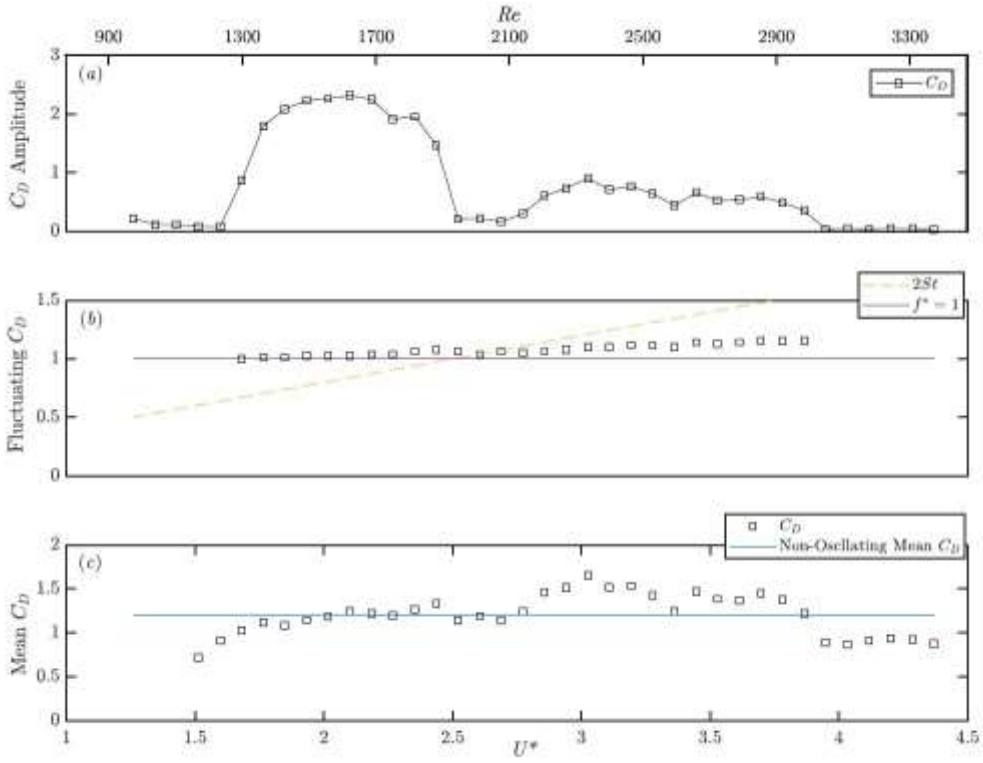

Figure 3: *(a)* Coefficient of the fluctuating drag, *(b)* frequency ratio of the fluctuating drag, and *(c)* coefficient of the mean drag value plotted against U^* and *Re*.

Also of interest in the general response is the phasing between the drag force and the cylinder displacement. As part of their study in streamwise flow perturbations, Konstantinidis and Balabani (2007) took advantage of the similarity in wake kinematics between forced- and free-oscillation studies to estimate the phasing between fluctuating drag and cylinder displacement at a reduced velocity of $U^* = 1.8$ (corresponding to a flow perturbation frequency of $f_e/f_{St} = 3$ in their study). They found the drag force and the displacement to be in phase with one another, in agreement with the results of a forced-oscillation study conducted by Nishihara *et al.* (2005). It should be mentioned that the fluctuating drag force used by Konstantinidis and Balabani (2007) was an estimated drag force, and not measured directly. Despite this, the values reported were still in agreement with experimental results of Nishihara *et al.* (2005).

The phase difference between the fluctuating drag and displacement based on the results of the present study is shown in figure 4. The phase difference was calculated by taking a small part of the time series at each reduced velocity and finding the time at which each signal crosses its respective mean. The time difference between this point for each signal is then used

to calculate the phase angle, which stays close to zero for the entire range of non-zero amplitudes. This finding extends the finding by Konstantinidis and Balabani (2007) to the entire lock-in region and implies a positive transfer of energy from the fluid to the structure throughout this region. As previously mentioned, the analysis by Konstantinidis and Balabani (2007) was performed only for U^* = 1.8. The results of this study show that this trend extends to all regions of response for the inline system.

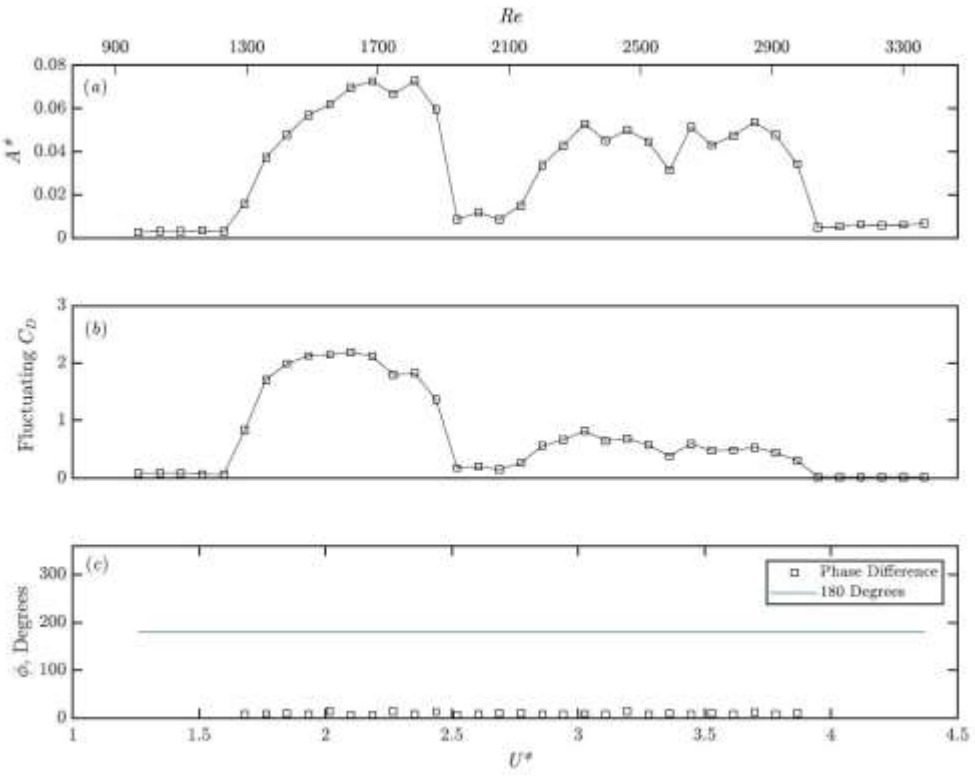

Figure 4: *(a)* Dimensionless displacement amplitude, *A**, *(b)* fluctuating C_D, and *(c)* phase difference between the two signals in degrees, plotted against *U** and *Re*. The phase difference of approximately 0 degrees corresponds to a positive transfer of energy from the fluid to the structure.

2.5 Flow Forces and Wake Modes

The existence of both symmetric and asymmetric shedding in the inline system has been discussed in previous studies both experimentally (Naudascher 1987; Okajima *et al*. 2002; Nishihara *et al*. 2005; Konstantinidis & Balabani 2007; Cagney & Balabani 2013a) and computationally (Al-Mdallal *et al.* 2007). There is general understanding that the initial regime of the first excitation region (approximately 1.6 < *U** < 2.2) is dominated by symmetric vortex

shedding, while the second excitation region (approximately $2.7 < U^* < 3.8$) is dominated by more typical (with regard to bluff body vortex shedding) asymmetric shedding.

Less certain is the behavior of the wake in the transition region (approximately $2.2 < U^* < 2.7$). In a study focused on understanding the wake behavior within this region, Cagney and Balabani (2013b) investigated mode competition in the wake of an in-line flexibly-mounted circular cylinder for a single parameter set with a true reduced velocity of $U^*St/f^* = 0.42$, corresponding to a reduced velocity of $U^* = 2.7$. Using PIV, they found that the symmetric (S-I) shedding mode was less stable than the asymmetric (A-II) mode for this reduced velocity. In 3000 velocity fields that were analyzed, the S-I mode was found in only 8% compared to 92% for the A-II mode. In a brief review of streamwise vibrations, Konstantinidis (2014) discussed this transition region between symmetric and asymmetric shedding. It was concluded based on available evidence that there is a coexistence between the two modes in this region.

The use of a very sensitive force sensor in the present study allows quantitative comparisons to be made between the forces present in the drag (streamwise) and lift (crossflow) directions. The relative magnitude of these forces gives direct insight into the type of shedding present for a given reduced velocity. The nature of the forces associated with typical asymmetric vortex shedding off of a circular cylinder are well understood (see Bearman 1984; Williamson and Govardhan 2004). Asymmetric vortices shed off of a fixed bluff body impart forces on that body in the lift direction at a frequency equal to the shedding frequency, f_{St}, (where one cycle of asymmetric shedding is defined as two subsequent vortices of opposite signs are shed from opposite sides of the body) and in the drag direction at a frequency equal to $2f_{St}$.

It follows from this logic that the presence of symmetric or asymmetric vortices can be determined by examining the magnitude ratios of the present lift and drag forces on the structure. The presence of symmetric vortices would result in crossflow, or lift, forces with a fluctuating magnitude of zero, or very close to zero relative to the magnitude of fluctuating drag. The lift force exerted by a symmetric vortex pair is negligible as two vortices are shed simultaneously from the two sides of the cylinder. Thus, in regions of reduced velocity where symmetric shedding is present, the ratio of the amplitudes of coefficient of fluctuating lift to coefficient of fluctuating drag, C_L/C_D ($C_L = 2F_L/U^2DL\rho$, where F_L is the fluctuating lift force), will be relatively low, as fluctuating drag forces dominate. In regions where asymmetric shedding is present, this ratio will be relatively large as fluctuating lift forces are introduced by the asymmetry of the wake.

This ratio of coefficients, $R_f = C_L/C_D$ is plotted as a function of reduced velocity in figure 5a. Dimensionless displacement as a function of reduced velocity is also re-plotted in figure 5b for reference. The ratio at each reduced velocity is plotted with a symbol that corresponds to the type of shedding that is present at that reduced velocity based on the ratio R_f, as well as the relative change in R_f with increasing reduced velocity. In the first region ($1.6 < U^* < 2.4$), the value of R_f is low and corresponds logically to symmetric shedding.

In addition, the values of R_f in this region remain low and do not change drastically with increasing reduced velocity. Previous forced-oscillation and oscillatory-flow studies (Al-Mdallal *et al.* 2007; Konstantinidis and Balabani 2007) have reported the existence of symmetric shedding with respect to a frequency ratio f_e/f_{St} or f_c/f_{St}. The response frequency of the self-excited vibrations of the system in the present study within this region, $1.6 < U^* < 2.4$, corresponds to a ratio of $2.46 < f/f_{St} < 3.2$. The points for low values of R_f are plotted in figure 5c against reduced velocity. The gradual increase in the value of R_f in this region indicates a gradual change in the nature of the symmetric shedding. This will be explored in greater details in Section 2.6.2.

Of particular interest is the region of reduced velocity of $2.4 < U^* < 2.9$. An increase in the value of R_f is observed at the start of this region, followed again by a drastic decrease in the ratio. For this reason, points within this region $2.4 < U^* < 2.9$ are said to be competitive with regard to their wake modes, in accordance with the argument proposed by Konstantinidis (2014). These points are said to be competitive primarily because of large and small values within this region. Compared to the regions for $U^* > 2.9$ and $U^* < 2.4$, the values of R_f fluctuate relative to one another.

Values of R_f for $U^* > 2.9$ are seen to stabilize at much larger values than those for $1.6 < U^* < 2.4$, and they correspond clearly to an asymmetric shedding pattern.

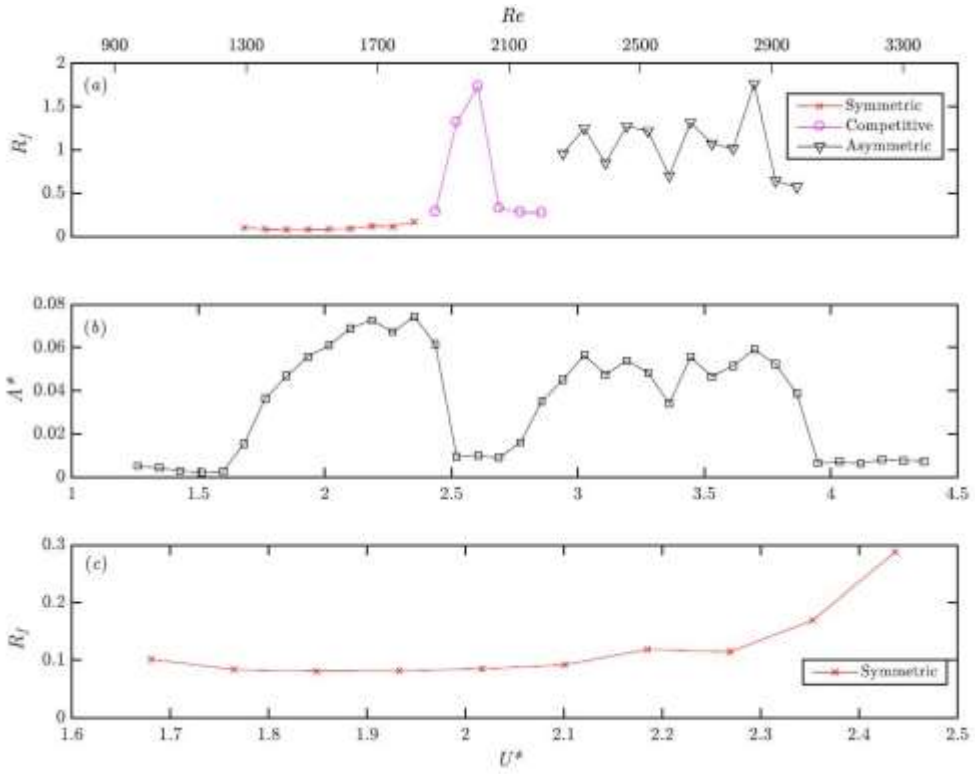

Figure 5: *(a)* The ratio of fluctuating lift to fluctuating drag, R_f and *(b)* the dimensionless amplitude of displacement plotted as a function of U^* and *Re*. Different symbols are used to indicate different wake modes depending on the values of R_f within the region. *(c)* The fluctuating force magnitude ratio, R_f, plotted against reduced velocity for the region of symmetric shedding (approximately $1.7 < U^* < 2.4$). The increase in the value of R_f towards the end of the region indicates a change in the nature of the symmetric wake mode.

The magnitudes of fluctuating C_L and C_D , their corresponding frequencies, and their mean values are plotted against reduced velocity, U^*, and Reynolds number, *Re*, in figure 6. Figure 6a shows that the magnitude of fluctuating lift increases over the range of reduced velocities tested. This is consistent with the wake mode of the inline system switching from symmetric to asymmetric as the reduced velocity is increased. The exception to this trend is within the region of competition (approximately $2.4 < U^* < 2.9$) where an exchange between the magnitude of the lift and drag coefficients takes place. The dimensionless frequencies of the fluctuating lift and drag can be seen in figure 6b. Both frequencies are made non-dimensional by dividing them by the system's natural frequency in otherwise still water (f_{nw}). In the reduced velocity range of $U^* > 2.4$, the fluctuating lift frequency, f_L, can be seen as approximately half of the fluctuating drag frequency, f_D, as expected for typical bluff body asymmetric vortex shedding. In the reduced velocity range of $U^* < 2.4$, the fluctuating lift frequency behaves rather curiously, being equal to that of the fluctuating drag frequency. However, this can be attributed to the nature of the experimental set up. Given the sensitivity of the force sensor, any

imperfection in the mounting of the cylinder to the force sensor, or the force sensor to the mounting plate (figure 1) results in a small but present contribution of the much larger fluctuating drag component in the lift direction, and therefore frequency contribution at the fluctuating drag frequency in the lift direction. The reduced velocity at which the fluctuating lift frequency becomes half of the fluctuating drag frequency corresponds to the end of symmetric shedding and the beginning of the region of competition between the symmetric and asymmetric patterns. The mean values of C_L and C_D are plotted in figure 6c. The mean value of C_L stays at approximately zero as expected for the entire range of reduced velocities. The mean value of C_D fluctuates slightly about a typical value for a fixed cylinder.

In order to provide an idea of the magnitudes of the dimensional forces that are measured in the present study, it should be mentioned that for the first response region (1.6 $< U^* <$ 2.5), the magnitude of the fluctuating drag force is approximately 25 mN. In the second response region, the fluctuating lift force reaches a magnitude of approximately 30 mN. These small magnitudes had made it impossible to measure forces of this system directly in the previous studies. This is overcome in the present study by using a very sensitive force sensor.

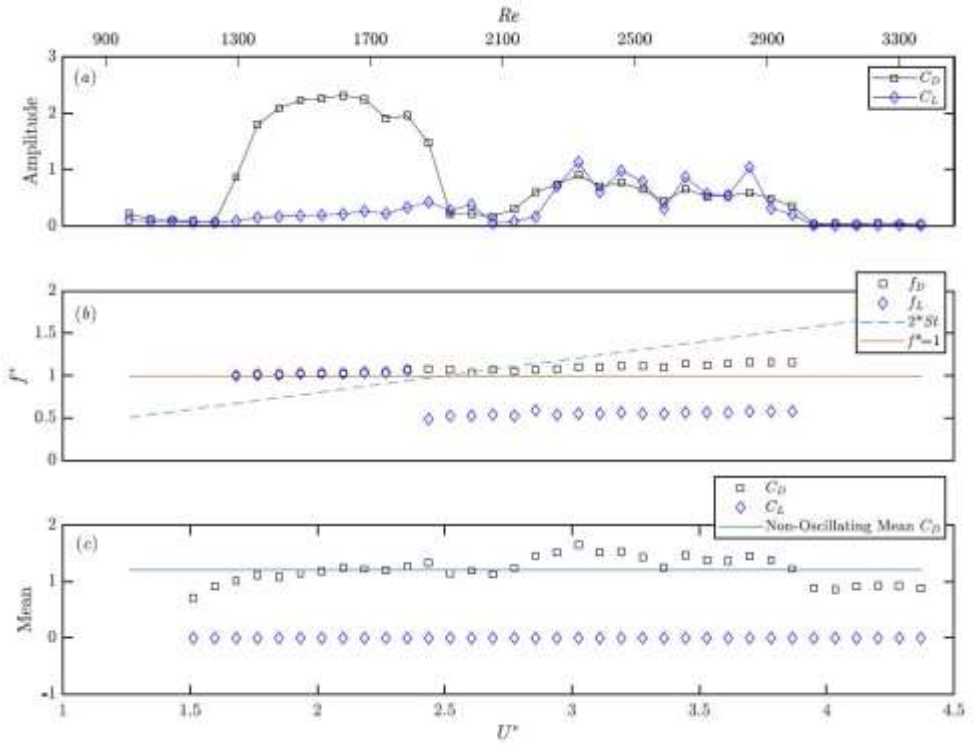

Figure 6: *(a)* The amplitude of fluctuating lift, C_L, and drag, C_D , *(b)* dimensionless frequency of fluctuating lift and drag, and *(c)* the mean value of C_L and C_D all plotted against U^* and *Re*.

2.6 Sample Responses

In this section, time histories of displacement, coefficients of lift and drag, and their respective spectral contents are examined for specific values of reduced velocity. Displacement and force time histories for all sample responses were filtered using a low pass filter set at 5 Hz to reduce signal noise. Flow visualization is also conducted at each reduced velocity. The time dependent force coefficients and their spectral contents are compared with flow visualizations to extend the discussions of previous sections.

2.6.1 Sample Response: U^*=2.1 – Symmetric S-I Shedding Mode

Figure 7 shows the time histories of dimensionless cylinder displacement and lift and drag coefficients together with their corresponding Fourier transforms for $U^* = 2.1$. Based on the Fourier transform of the coefficients of drag and lift, symmetric shedding is expected to be present for this reduced velocity, as Figure 7d shows that there is no peak in the lift coefficient at a frequency of one half f_{nw}. A peak at one half f_{nw} would indicate asymmetry in the immediate wake of the cylinder.

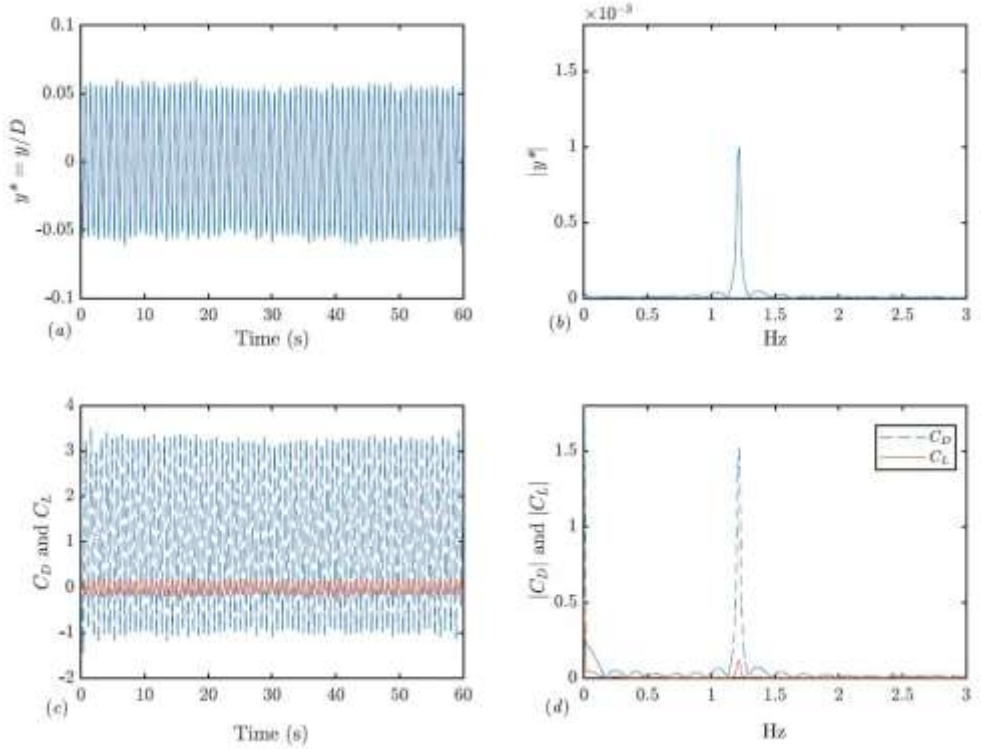

Figure 7: Time histories of the *(a)* dimensionless displacement, and *(b)* coefficients of fluctuating lift and drag together with the frequency contents of *(c)* displacement, and *(d)* fluctuating lift and drag, all for $U^* = 2.1$. Bumps in the frequency contents at low frequencies are artifacts of analyzing a relatively weak signal.

A symmetric shedding mode is expected for $U^*= 2.1$ based on the results of previous research (Aguirre 1977; Naudascher 1987; Okajima et al. 2002; Cagney & Balabani 2013a) and thus the results for force coefficients are consistent with previous studies. Flow visualization was also conducted for this reduced velocity to confirm and complement the results of the force data. A view of the immediate wake can be seen in figure 8. The images in figure 8 (and also later in figures 10, 12, and 14) are presented sequentially over nine periods of oscillations, at time steps of approximately 0.84 s, which corresponds to the period of oscillations. Nine oscillations are shown to provide a more definitive view of the wake. A video of the wake at this reduced velocity is available online. According to wake classifications that have been applied to the streamwise circular cylinder in previous studies (Cagney and Balabani 2013a), the wake in this region exhibits an S-I shedding mode, in which one pair of symmetric vortices is shed per cycle of oscillations. While the wake may rearrange itself downstream into an asymmetric pattern, the cylinder does not feel this asymmetry as indicated in the fluctuating lift and drag frequency plots of figure 7d.

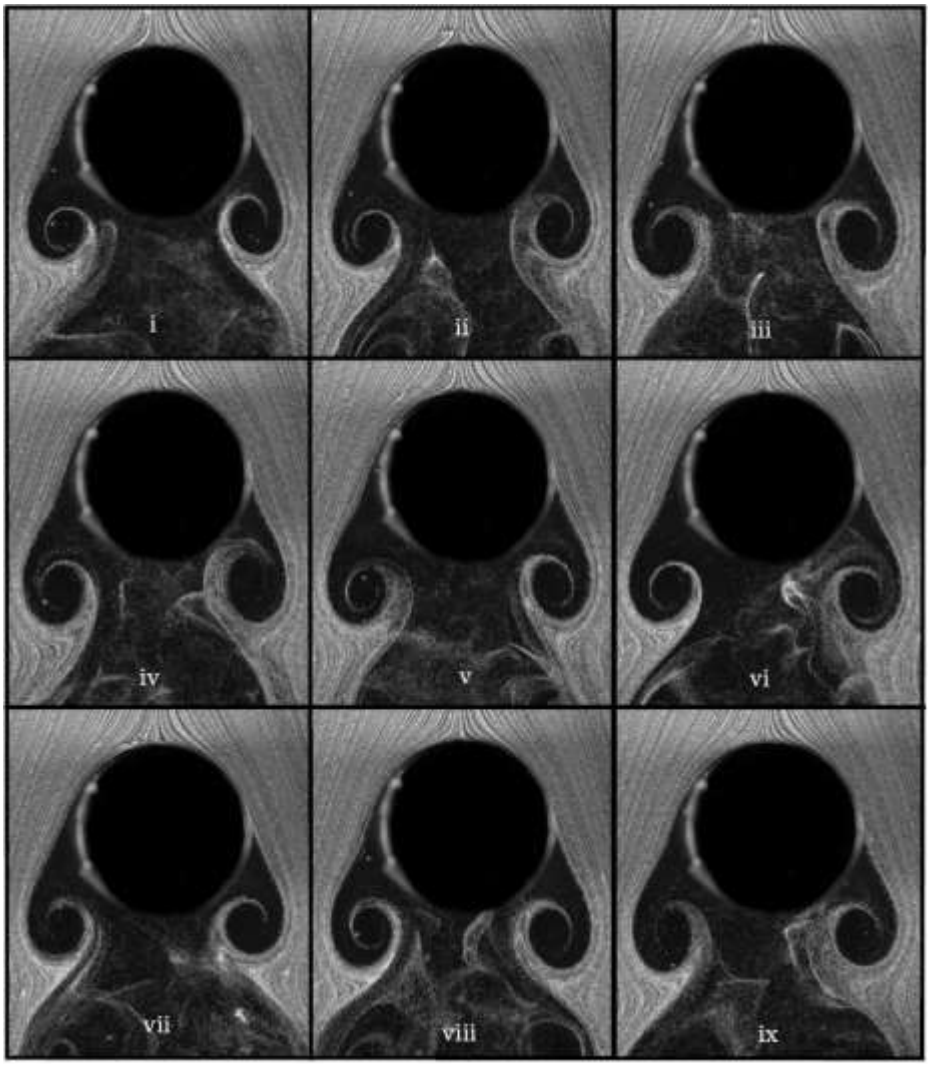

Figure 8: Symmetric S-I shedding shown for U^* = 2.1. Flow is from top to bottom.

2.6.2 Sample Response: U^*=2.27 – Alternating Symmetric (AS) shedding mode

Figure 9 shows the same plots as those in figure 7 but for U^* = 2.27. The frequency contents of the fluctuating lift as seen in figure 9d now contain a small but present peak at a value of $f_{nw}/2$. Note that the dominant force on the cylinder for this reduced velocity remains to be the fluctuating drag at a frequency equal to the response frequency and f_{nw}. It follows from this that the vortex shedding in this region still consists of two vortices of opposite signs being shed simultaneously from the two sides of the cylinder, yet the frequency contents of the lift coefficient suggest a certain degree of asymmetry. This change in the coefficient of fluctuating lift was also seen, although not discussed, by Nishihara *et al.* (2005). In figure 5 of Nishihara *et al.* (2005), the magnitude of the coefficient of fluctuating lift can be seen to change dramatically

between a reduced velocity of $U^* = 1.7$ and $U^* = 2.2$. If a spectral analysis had been done on the signal, the same peak at $f_{nw}/2$ should have been observed. In their case this would have occurred at $f/2$ (where f is the frequency of forced oscillations).

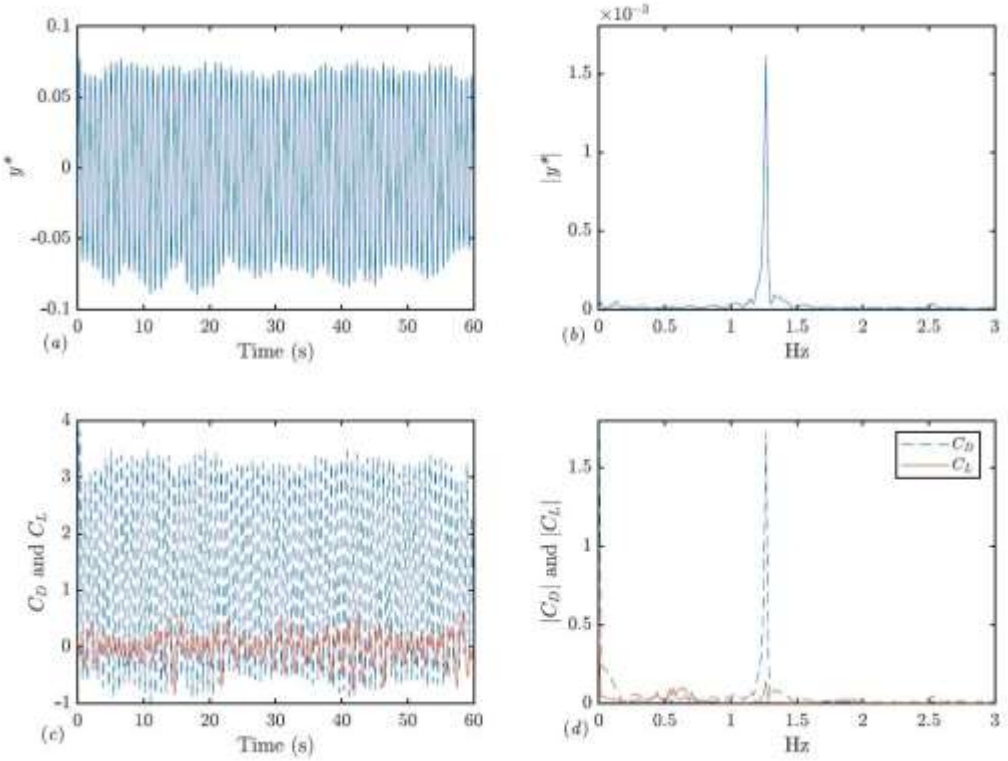

Figure 9: Time histories of the *(a)* dimensionless displacement, and *(b)* coefficients of fluctuating lift and drag together with the frequency contents of *(c)* displacement, and *(d)* fluctuating lift and drag, all for $U^* = 2.27$.

The immediate wake for this reduced velocity is shown in figure 10. A video of the wake at this reduced velocity is also available online and provides very clear view of the wake mode described in this section. The shedding mode for this reduced velocity exhibits elements of both symmetric and asymmetric modes that had not been classified before. The wake is symmetric because the shedding still consists of two vortices of opposite signs being shed simultaneously from the two sides of the cylinder. However, the vortices are no longer of the same size (when compared to the case of $U^* = 2.1$) and alternate in size for each cycle of shedding.

For the near wake, this type of shedding has not been observed in previous studies and we will call this the Alternating-Symmetric (AS) mode, in which two vortices of opposite signs are shed simultaneously per cycle of shedding, but alternate in size relative to one another.

This is not to be confused with the SA (Streamwise Antisymmetric) mode described by Jauvtis and Williamson (2004) in which one vortex is shed per cycle, alternating vorticity every cycle, at the centerline of the structure. The resulting wake at this reduced velocity confirms the prediction made in figure 5c, in which the nature of symmetric shedding was shown to change when examining the ratio R_f. The resulting AS wake in this region corresponds to $R_f = 0.115$. The AS mode exists briefly in the reduced velocity range of $2.19 < U^* < 2.36$, corresponding to $0.115 < R_f < 0.169$. In this region, forces on the structure are still dominated by fluctuating drag forces, but a non-trivial magnitude of fluctuating lift begins to appear as the wake transitions away from symmetry.

This has been confirmed by observing time histories and flow visualizations for the reduced velocity range of $2.19 < U^* < 2.36$. Within this range, the magnitude of the fluctuating lift coefficient is larger than that for $U^* < 2.19$, and contains a frequency peak at $f_{nw}/2$. In addition, flow visualization has been conducted and the presence of the AS shedding mode has been confirmed for $2.19 < U^* < 2.36$.

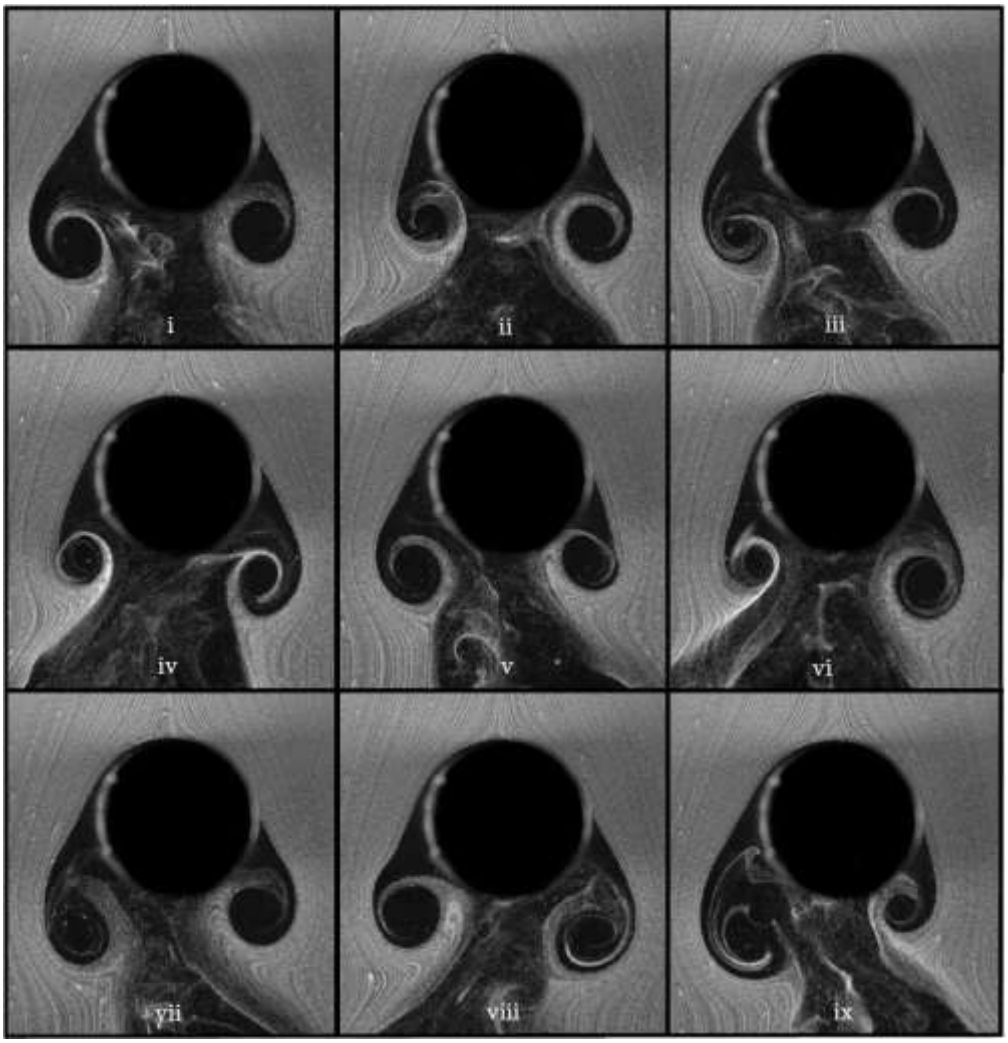

Figure 10: Alternating-Symmetric AS shedding shown for U^* = 2.27. Flow is from top to bottom.

2.6.3 Sample Response: U^*=2.77 – Weak and competitive shedding

Figure 11 shows the same plots as figures 7 and 9 but for U^* = 2.77. The response of the system for this value of reduced velocity has now changed dramatically, as it is within the region of lowest-amplitude response. Note that the range of the *y*-axis of figure 11d has been changed compared to figures 7d and 9d so that the relatively weaker peaks are easier to observe. The time histories of both the coefficients of lift and drag suggest that this is a region of competition with regard to wake modes, as neither maintain a steady magnitude.

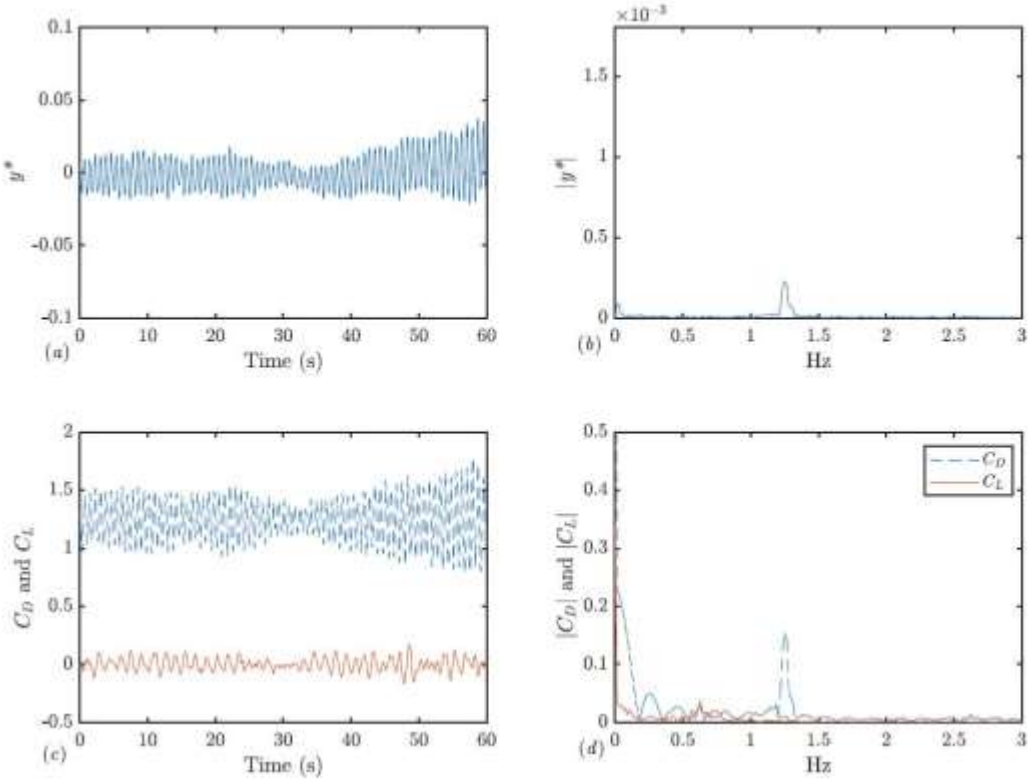

Figure 11: Time histories of the *(a)* dimensionless displacement, and *(b)* coefficients of fluctuating lift and drag together with the frequency contents of *(c)* displacement, and *(d)* fluctuating lift and drag, all for $U^* = 2.77$.

The immediate wake for this reduced velocity is shown in figure 12. The wake for this region exhibits a particularly non-distinct and weak shedding pattern. The snapshots of the wake also show the presence of vortex structures resembling both symmetric and asymmetric shedding modes. This follows the findings of Cagney and Balabani (2013b) as well as the arguments made in the review by Konstantinidis (2014) in which it is argued that competition and a coexistence of symmetric and asymmetric modes exist in this region. A video of the wake at this reduced velocity is available online.

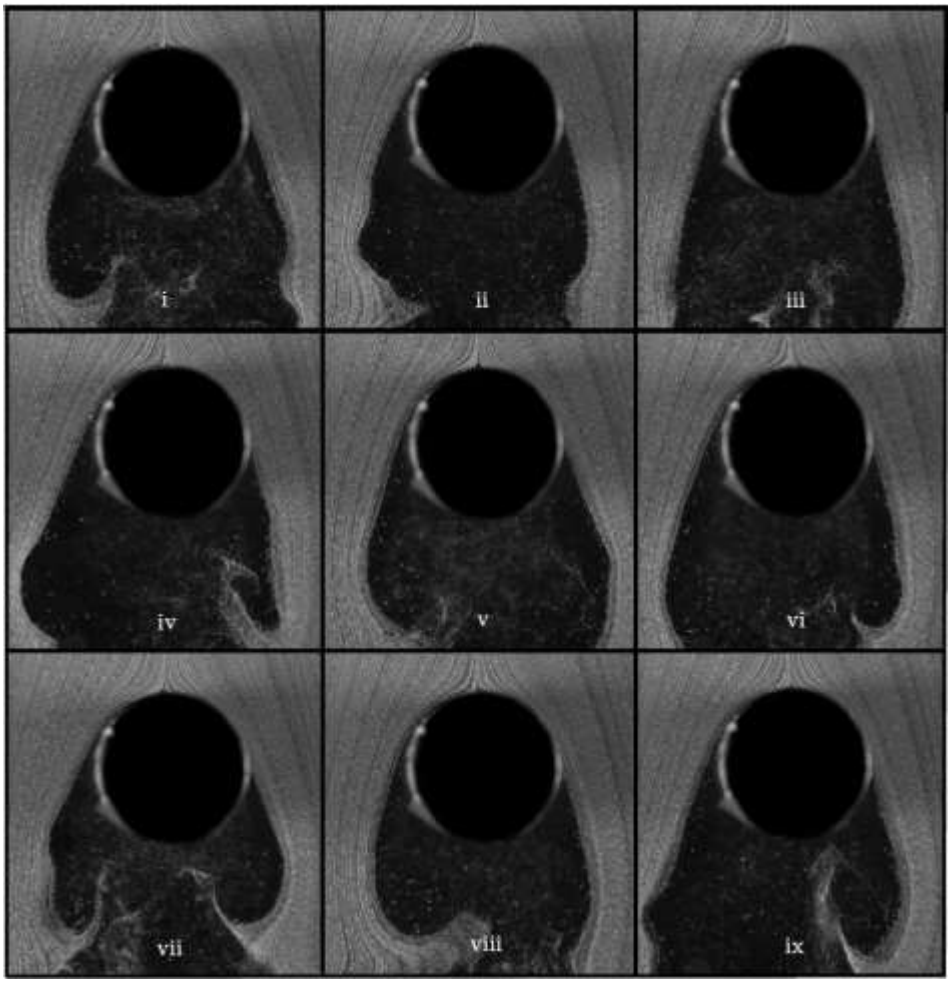

Figure 12: Weak and competitive shedding shown for U^* = 2.77. Flow is from top to bottom.

2.6.4 Sample Response: U^*=3.45 – Streamwise Asymmetric (SA) shedding mode

Figure 13 shows the same plots as those in figures 7, 9, and 11 but for U^* = 3.45. The time histories for this reduced velocity confirm the presence of fully developed asymmetric shedding, consistent with previous studies (Aguirre 1977; Naudascher 1987; Okajima *et al*. 2002; Cagney & Balabani 2013a). A well-defined peak at $f_{nw}/2$ can be seen in figure 13d for the fluctuating lift, consistent with the forces that are expected for asymmetric shedding. In the drag direction, a frequency double that of the lift, and equal to f_{nw} is observed. While the presence and quantitative nature of the lift forces give insight into the wake mode, fluctuating drag forces are the only ones that provide excitation to the structure. The frequencies of fluctuating lift and drag forces imply an asymmetric shedding frequency equal to $f_{nw}/2$, with two vortices being shed from opposite sides of the cylinder per cycle of shedding.

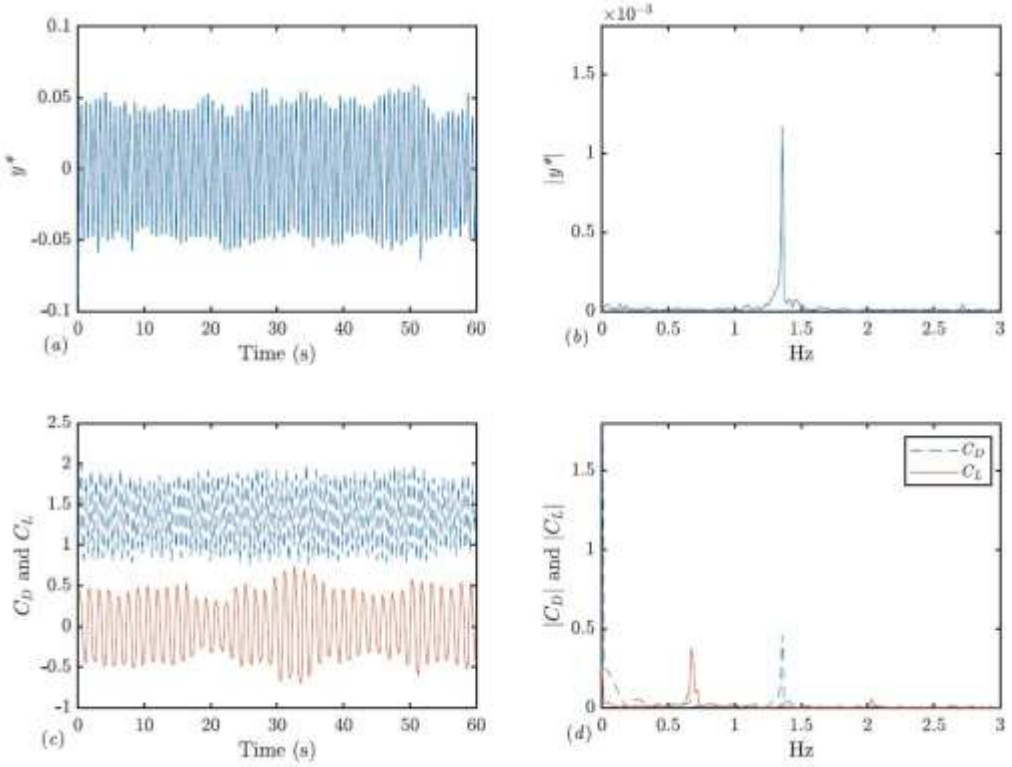

Figure 13: Time histories of the *(a)* dimensionless displacement, and *(b)* coefficients of fluctuating lift and drag together with the frequency contents of *(c)* displacement, and *(d)* fluctuating lift and drag, all for $U^* = 3.45$.

As with previous cases, flow visualization was used at this reduced velocity to further investigate the wake. The result is a clear case of "SA" shedding, as described by Jauvtis and Williamson (2004), in which a vortex is shed from each side of the cylinder per cycle of shedding on the center line of the structure. The flow visualization for $U^* = 3.45$ can be seen in Figure 14. A video of the wake visualization at for this reduced velocity can be found online.

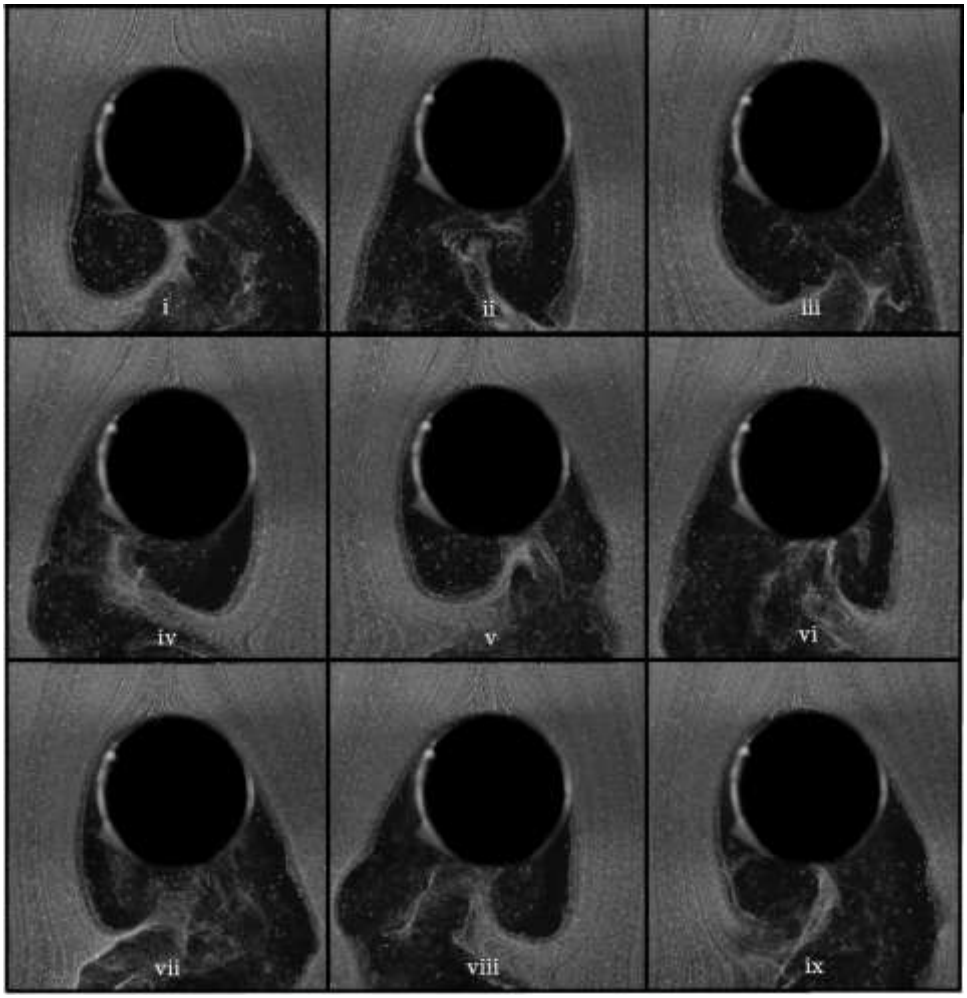

Figure 14: SA (Jauvtis and Williamson 2004) asymmetric shedding mode shown for U^* = 3.45. Flow is from top to bottom.

CHAPTER 3

SQUARE PRISM

3.1 Experimental Set Up

A square prism with a side length of D = 19.05 mm (where D is the side length of the square cross section) and a submerged length of L = 386 mm corresponding to an aspect ratio of 20 was also tested in the same recirculating water tunnel used for the experiments in Chapter 2. The cylinder was made of 3D printed plastic with a wall thickness of 1.016 mm. This thickness ensured the cross section was rigid and lightweight. The section was sealed to ensure that none of the surrounding fluid would find its way into the hollow section. The cylinder was mounted on the same air bearing system as described in Section 2.1 (see figure 1). The structural damping ratio was measured experimentally using a decay test in air and was found to be ζ = 0.008. Springs were attached from the mount plate on the air bearings to a fixed mounting point. The mass ratio for the square prism was m^* = 1.72. The moving mass accounted for the mass of every component that was moving with the prism, including the force sensor, air bearings, mount plate, and 3D-printed adapter.

3.2 Flow Quality

A recirculating water tunnel with the test-section dimensions of 1.27 m x 0.5 m x 0.38 m was used for this series of experiments. To ensure uniform flow and accurate velocity, bubble image velocimetry (BIV) was used to obtain flow profiles at varying test-section depths. The details of this procedure are documented in Seyed-Aghazadeh *et al.* (2017).

3.3 Data Collection

Data were collected for the square prism experiments using the same sensors and precautions as with the circular cylinder. Using a decay test in water, the system's natural frequency in water, f_{nw}, was found to be 0.915 Hz.

Displacement and force data were captured at each angle of incidence (see Table 1) over a range of flow velocities. Experiments were started at a flow velocity of 0.04 m/s and the flow velocity was increased in increments of 0.007 m/s up to 0.1 m/s at each angle of incidence. This corresponds to a Reynolds number range of $757 < Re < 1900$ and reduced velocity range of $2.4 < U^* < 5.8$.

Table 1: All angles of incidence tested in this study.

Angle of Incidence, α
0°
2.5°
5°
7.5°
10°
13.5°
16°
20°
25°
30°
35°
40°
45°

Force and displacement data were collected for 120 seconds at each flow velocity. The data from the force sensor were collected in tandem with those of the displacement sensor so that the respective time histories were synchronized. The definition of angle of incidence as used in this chapter can be seen in figure 15.

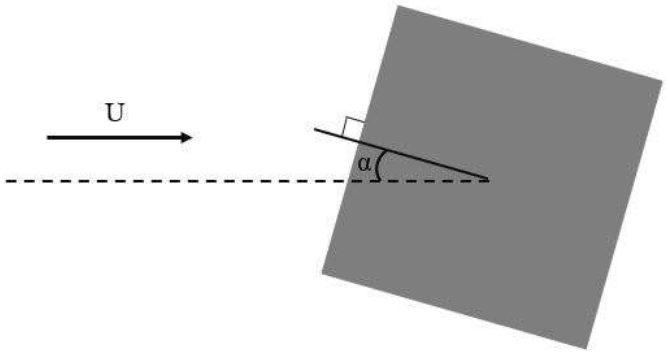

Figure 15: Angle of incidence, α, as defined in this paper.

Hydrogen bubble generation was used for flow visualization, just as it was for the circular cylinder. A detailed description of the system used for hydrogen bubble generation is documented in Seyed-Aghazadeh *et al.* (2017). The wake images were captured using a Phantom Miro M110 high speed camera.

3.4. The Strouhal Law for a Square Prism

Defining the non-dimensional frequency of vortex shedding for a square prism requires more care then for a shape such as a circular cylinder. This is because the Strouhal number, *St*, is a function of not only the cross section, but the angle of incidence, α. Multiple studies (Obasaju 1984; Naudascher 1987; Knisley 1990) have investigated this trend, which is summarized below in figure 16. The plot includes the results of past studies, but also an average the curve, the values of which are used in the present study.

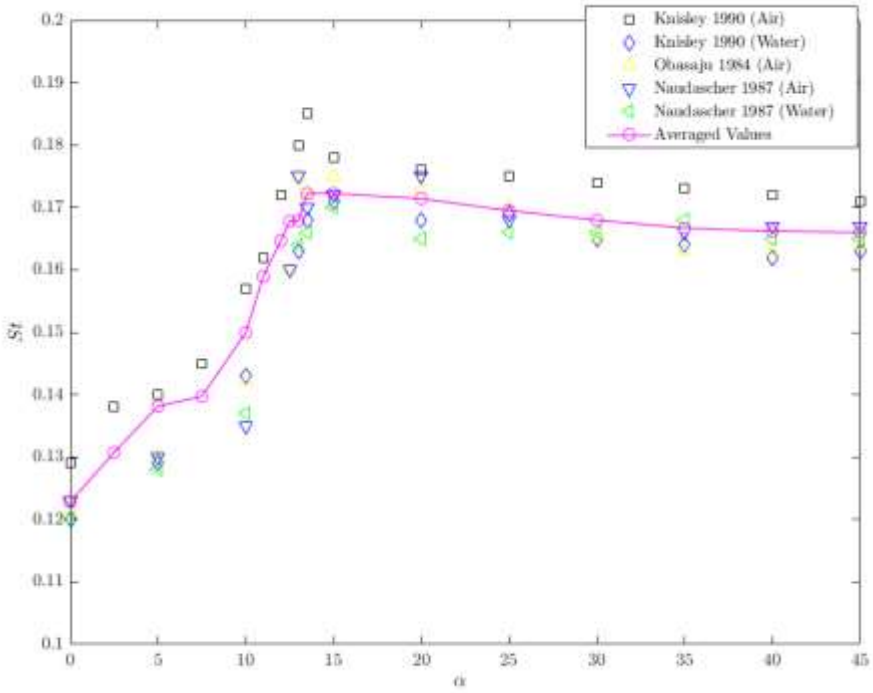

Figure 16: *St* plotted against angle of incidence, α, for multiple studies with an average value curve.

The average curve was created by summing the data points provided for each α by previous studies and dividing each value by the number of points present at that α. For example, only one previous study conducted tests for *St* at α = 2.5°, but all conducted tests for *St* at α = 30°. The curve was then smoothed using a 3-point moving average.

3.5 The General Behavior of the Cylinder

The displacment response of the square cylinder system is highly dependent on angle of incidence and can be seen figure 17. When the cylinder is angled such that it behaves as a symmetric system ($\alpha = 0°$) it exhibits a significant displacement response from $3.2 < U^* < 5.4$. The general trend with increasing angle of incidence is for the response amplitude to decrease and for the range of reduced velocity over which a response exists to also decrease. At an angle of incidence $\alpha = 10°$ the response dissapears entirely. This finding is very consistent with those of Naudascher (1987). This finding is also consistent with the existence of a critical $\alpha = 13.5$, which is discussed by Rockwell (1977) and can also be seen in St as a function of α in figure 16. It appears that the response of the system changes quickly as the angle of incidence, α, increases towards the critical α. For angles of incidence $\alpha = 0°, 2.5°, 5°, 7.5°$, a significant displacement response exists.

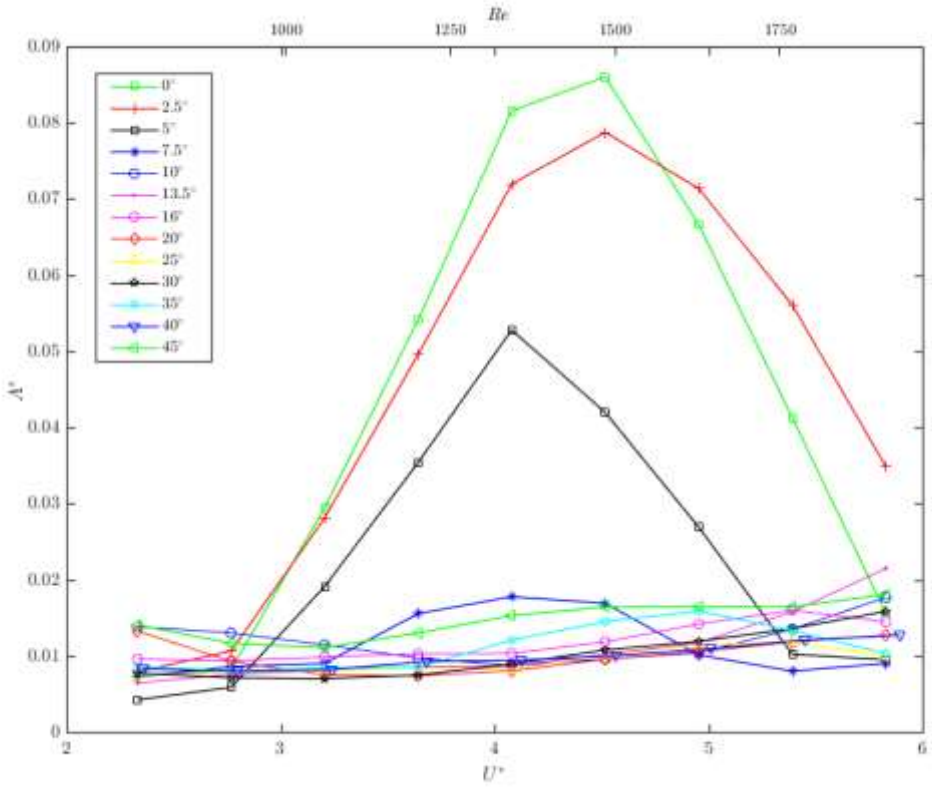

Figure 17: Dimensionless displacement amplitude, A^*, as a function of reduced velocity, U^*, and Reynolds number, Re, for the current study at all angles of incidence.

The tendency of the displacement response to decrease in width and magnitude with increasing angle of incidence can be seen from an alternative perspective in the surface plot shown in figure 18. The plot uses a log scale y-axis so that the details of the response at low angles of attack can be better observed. The decrease in width of the response region is highly evident in figure 18.

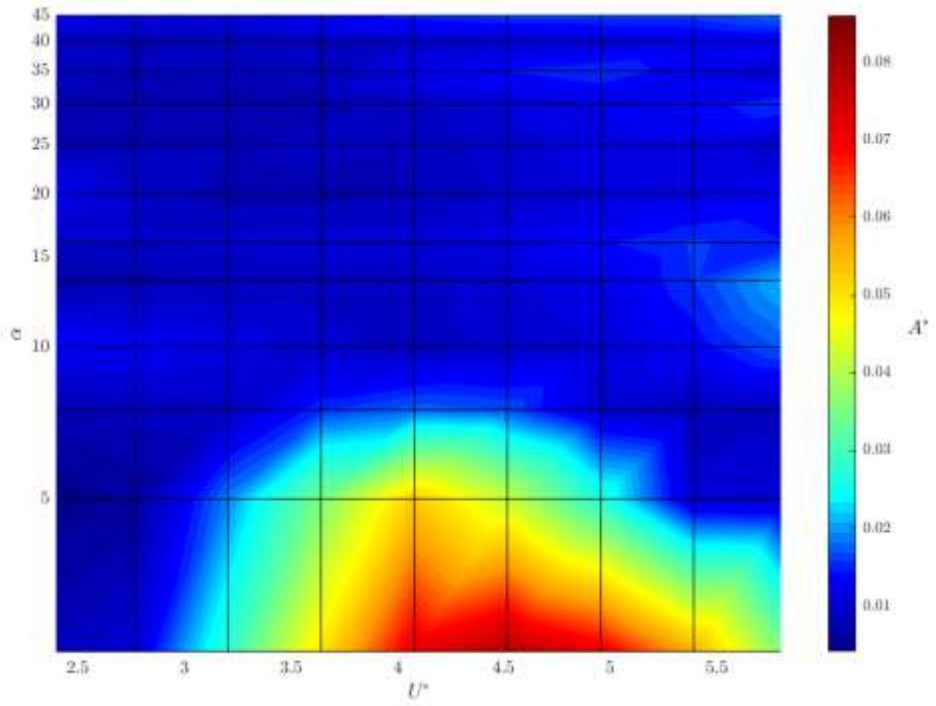

Figure 18: Surface plot of dimensionless displacement, A^*, shown as a function of reduced velocity, U^*, and angle of incidence α.

The question of whether the system is exhibiting a lock in response over the region shown in figure 18 can be investigated by looking at the forces in the drag direction over the region of response. Specifically, figure 19 shows the amplitude of the fluctuating coefficient of drag, C_D, as a function of reduced velocity, U^*. As with the circular cylinder, inertial forces associated with the accelerations present in the displacement response have been removed in post processing and do not contribute to the fluctuating C_D amplitude shown. The trends that exist in C_D are markedly similar those that exist in the displacement response. With increasing α, the magnitude of fluctuating C_D tends to decrease, while the range of reduced velocity over which a significant response exists also shrinks.

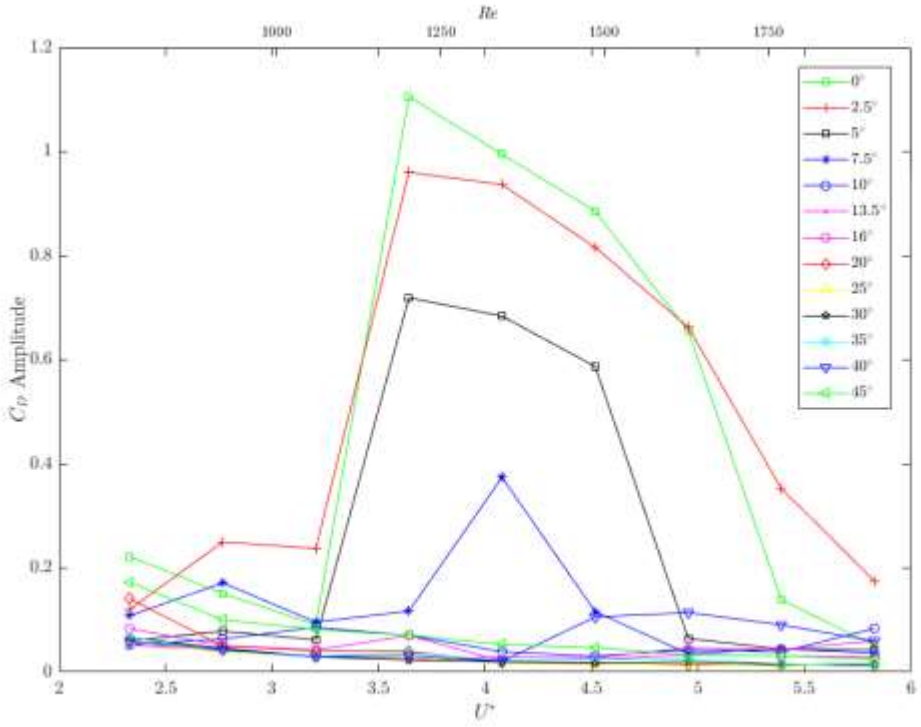

Figure 19: Fluctuating coefficient of drag, C_D, as a function of reduced velocity, U^*, and Reynolds number, Re, at all angles of incidence.

A surface plot of this data can be seen in figure 20. As in the 2D plot, figure 20 and figure 18 follow a very similar trend. This is an expected result. A large displacement response merits that the flow forces be larger for those reduced velocities. Figure 20 also shows angle of incidence, α, on the y-axis on a log scale so that the details of the force data can be observed more readily for those angles of incidence where a response exists.

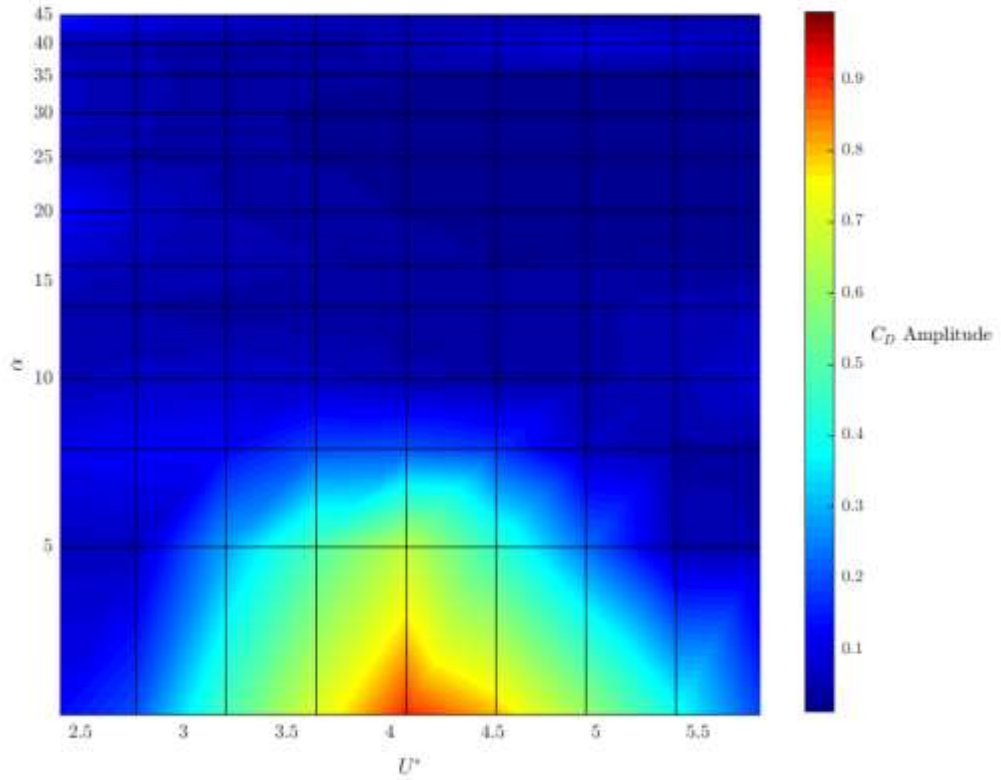

Figure 20: Surface plot of fluctuating coefficient of drag, C_D, amplitude shown as a function of reduced velocity, U^*, and angle of incidence α.

The similarities present in the displacement and fluctuating C_D response of the square prism are not necessarily indicative of lock-in. To further characterize this response, the frequencies of both must be observed. The definition of lock-in is a region of reduced velocity, U^*, (changed in this study by changing the flow velocity) over which the frequency of oscillations and vortex shedding synchronize with one another such that the vortex shedding ceases to increase linearly with flow velocity (according to the Strouhal law). Since the inertial forces have been removed from the force time histories, the frequency associated with fluctuating drag must only be associated with flow forces on the structure, and thus the vortex shedding.

The displacement frequency response for the 4 angles of incidence at which a response exists, α = 0°, 2.5°, 5°, 7.5° can be seen in figure 21e, f g and h respectively. For each frequency response, two times the Strouhal frequency, *St*, is plotted as a function of U^*. The reason for plotting two times the frequency is the same as for the circular cylinder. Namely, typical asymmetric vortices exert force in the drag direction at double the frequency that they exert

force in the lift direction. Any lock-in region would be expected to begin at a point where 2 times *St* intersected with the natural frequency of the structure.

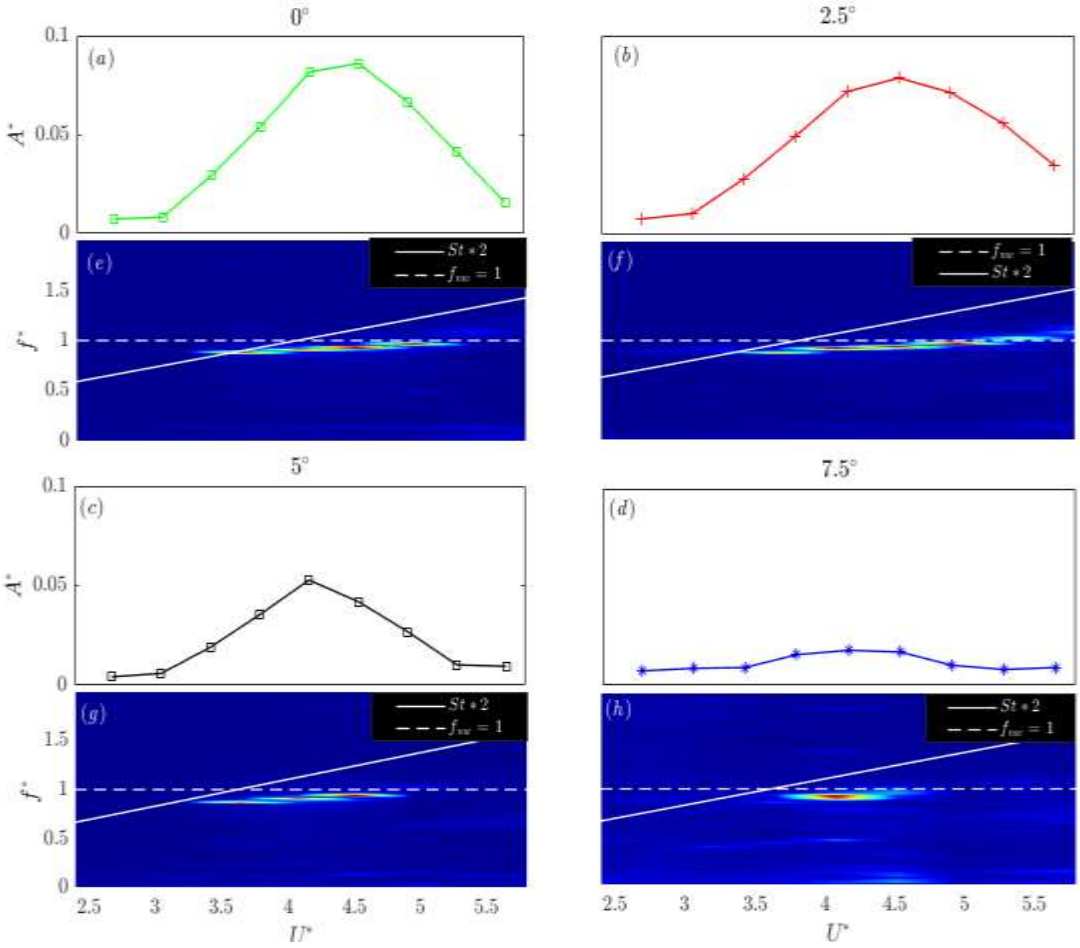

Figure 21: *(a), (b), (c), (d),* dimensionless amplitude of displacement, *A**, for α = 0°, 2.5°, 5°, 7.5° respectively. *(e), (f), (g), (h),* dimensionless displacement frequency response, *f**, for α = 0°, 2.5°, 5°, 7.5° respectively.

For each angle of incidence, the beginning of the region of response correlates well with the intersection of 2**St* and *f* = 1.* The surface intensity in figure 21e, f, g and h are presented here as relative values. The dominant frequency for each displacement response is shown to be near equal to the natural frequency of the system, f_{nw}, and remains constant over the range of *U** for which there is a displacement response.

The frequency of fluctuating C_D is shown in figure 22 for the same angles of incidence plotted in figure 21. A comparison between these two figures allows the conclusion that the square prism remains locked-in over the entire *U** range at all values of α for which there is a displacement response. The dominant frequency of fluctuating C_D remains constant and approximately equal to f_{nw} for each value of α over the entire *U** range for which there is a

displacement response. The combination of displacement and force frequency responses implies that both the vortex shedding frequency and structure natural frequency are synchronized over the region of response. Thus, the structure is locked in.

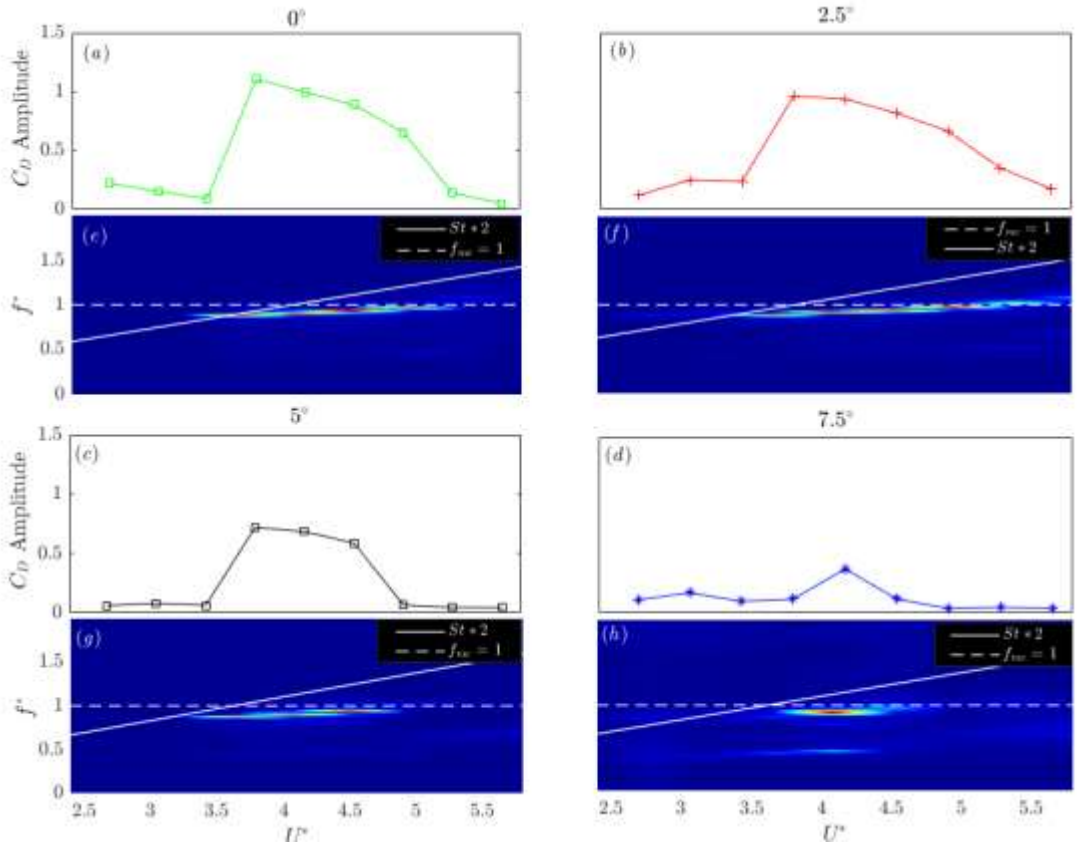

Figure 22: *(a), (b), (c), (d),* amplitude of fluctuating coefficient of drag, C_D, for α = 0°, 2.5°, 5°, 7.5° respectively. *(e), (f), (g), (h),* dimensionless C_D frequency response, f^*, for α = 0°, 2.5°, 5°, 7.5° respectively.

Figure 22h also shows a non-trivial contribution of $f_{nw}/2$ in the frequency response. This is understandable, as the increased angle of incidence allows the lift forces (which are occurring at half the frequency of the drag forces) to be translated into the drag direction.

Also of interest in the general response is the phasing between the drag force and the cylinder displacement. The phase difference was calculated by taking a small part of the time series at each reduced velocity and finding the time at which each signal crosses its respective mean. The time difference between this point for each signal is then used to calculate the phase angle. This phase angle is shown in figure 23 for angles of incidence α = 0°, 2.5°, 5°, 7.5° (angles for which there is a significant response). For all values of U^* at which a significant displacement exists the phase difference, φ, remains close to 0°. This result implies a positive

transfer of energy from the fluid to the structure at values of U^* for which there is significnat response.

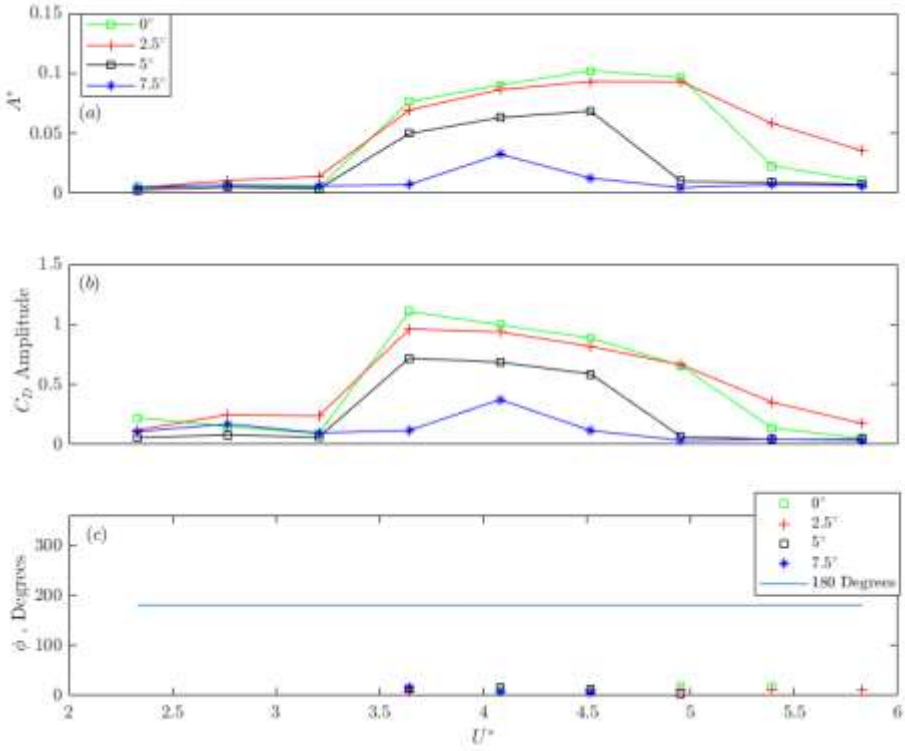

Figure 23: *(a)* Dimensionless displacement amplitude, *A**, *(b)* fluctuating C_D, and *(c)* phase difference between the two signals in degrees, plotted against *U**. The phase difference of approximately 0 degrees corresponds to a positive transfer of energy from the fluid to the structure.

3.6 Sample Responses

In this section, time histories of displacement, coefficients of lift and drag, and their spectral contents are examined for two specific cases. The signals were filtered using a low pass filter set at 5Hz to reduce signal noise. Flow visualization is observed in both cases, and connections are drawn between the time histories and observed wake structures.

3.6.1 Sample Response: α = 0°, *U** = 4.1

Figure 24 shows the time history of dimensionless cylinder displacement and drag and lift coefficients together with their corresponding frequency contents for α = 0° and *U** = 4. The spectral contents of the coefficients of lift and drag imply the presence of primarily symmetric

shedding. A significant peak in the spectral content of C_L at $f_{nw}/2$ in figure 24d would indicate a degree of asymmetry in the immediate wake of the cylinder. However, a small peak does exist. This suggests that while the shedding is primarily symmetric, its symmetry is not as uniform as the wake described in section 2.6.1.

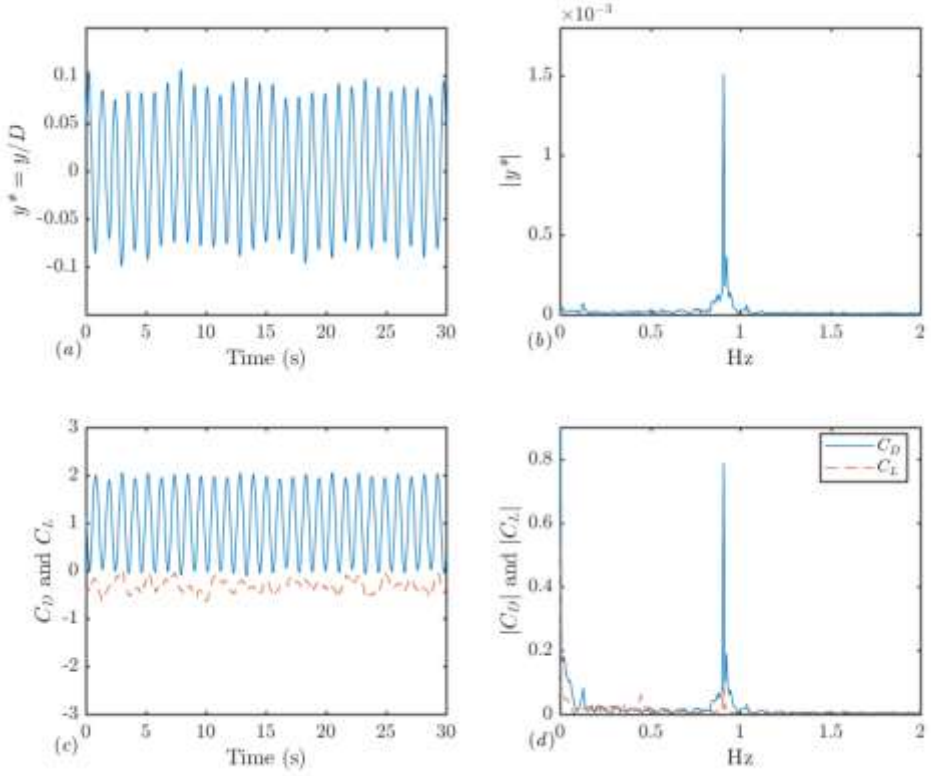

Figure 24: Time histories of the *(a)* dimensionless displacement, and *(b)* coefficients of fluctuating lift and drag together with the frequency contents of *(c)* displacement, and *(d)* fluctuating lift and drag, all for $\alpha = 0°$ and $U^* = 4.1$.

For this set of a parameters, a symmetric shedding mode is expected. Naudascher (1987) presented wake images of a square prism for these parameters and observed the presence of symmetric vortices, in which two vortices of opposite sign were shed per cycle of oscillation. Flow visualization was conducted for this reduced velocity to confirm what is suggested in figure 24. A view of the immediate wake for this parameter set can be seen in figure 25. The images in figure 25 (and also later in figure 27) are presented sequentially over nine periods of oscillation, at time steps of approximately $1/f_{nw} = 1.1$ s. The wake shown in figure 25 does in fact agree with the time histories and the findings of Naudascher (1987) and shows a symmetric shedding pattern. However, it should be noted that these symmetric structures are far less

ordered and laminar than those observed and described in the wake of the circular cylinder. This degree of asymmetry can be seen in the time history of C_L in figure 24c and d.

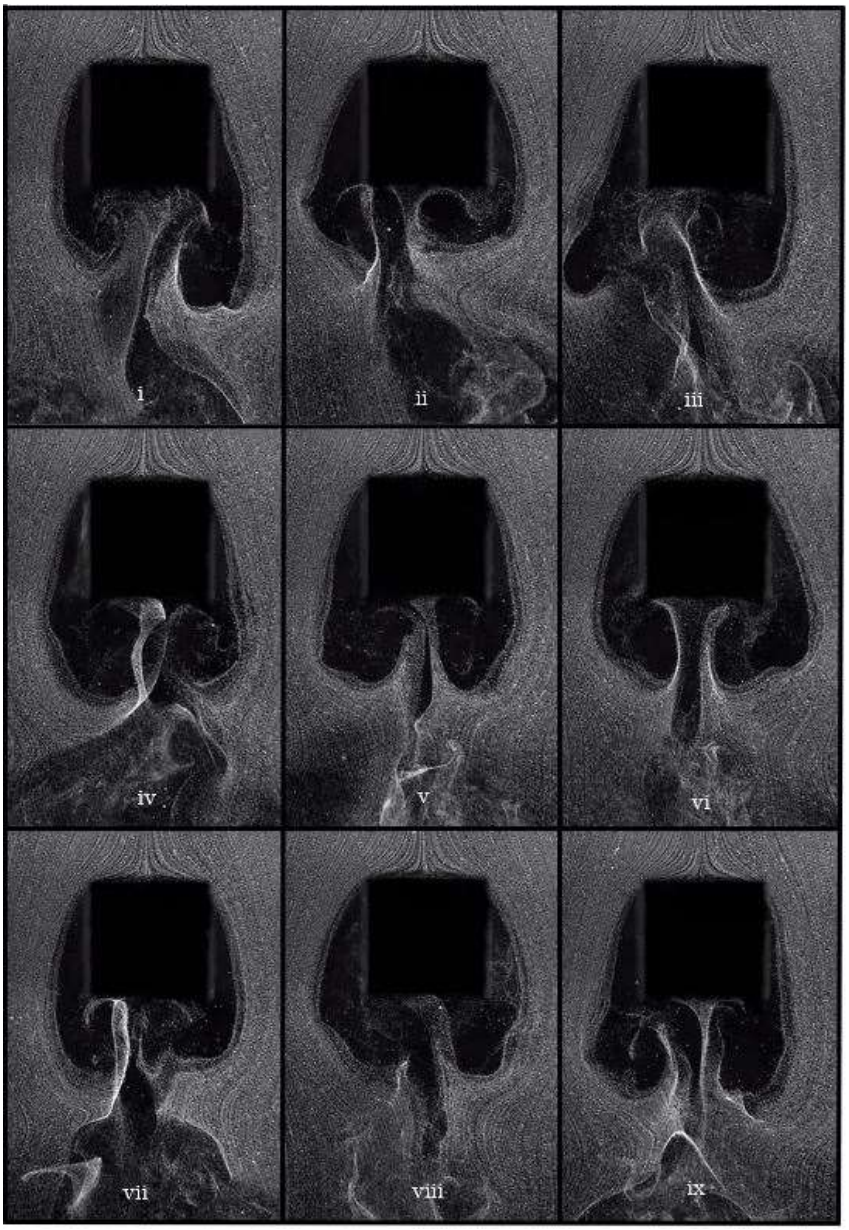

Figure 25: Rough symmetric shedding for U^* = 4, α = 0°

3.6.2 Sample Response: α = 5°, U^* = 4.1

Figure 26 shows the same plots as those in figure 24 but for α = 5° and = 4. The frequency contents of the fluctuating lift as seen in figure 26d now contain a small but present

peak at a value of $f_{nw}/2$. Note that the dominant force on the cylinder for this parameter set remains to be the fluctuating drag at a frequency equal to the response frequency and f_{nw}. It follows from this that the vortex shedding in this region still consists a primarily symmetric structure, yet the frequency contents of the lift coefficient suggest a certain degree of asymmetry.

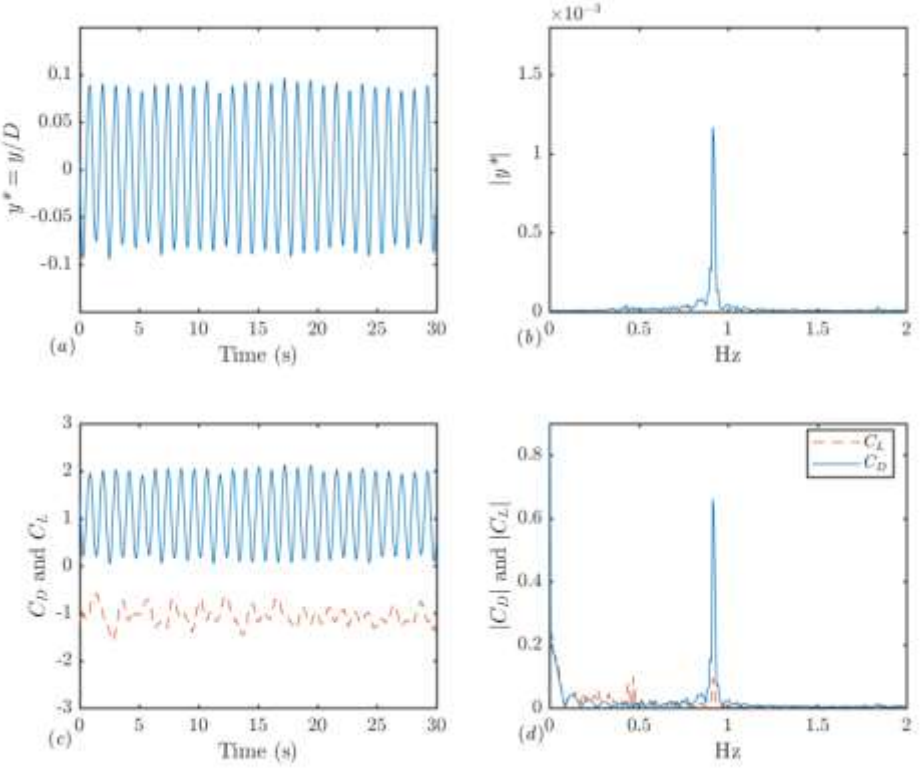

Figure 26: Time histories of the *(a)* dimensionless displacement, and *(b)* coefficients of fluctuating lift and drag together with the frequency contents of *(c)* displacement, and *(d)* fluctuating lift and drag, all for $\alpha = 5°$ and $U^* = 4.1$.

Due to the passive asymmetry present at an angle of incidence $\alpha = 5°$, it is also possible that completely symmetric wake structures could impart a small impulse on the structure in the lift direction. However, the frequency of this impulse would be at the vortex shedding (and oscillation) frequency, as supposed to a value $f_{nw}/2$. A peak at both f_{nw} and $f_{nw}/2$ can be seen in figure 26d, and so the data implies a certain amount of asymmetry in the wake in addition to the passive asymmetry of the structure. The immediate wake for this parameter set can be seen in figure 27. The structures observed are consistent with the data seen figure 26.

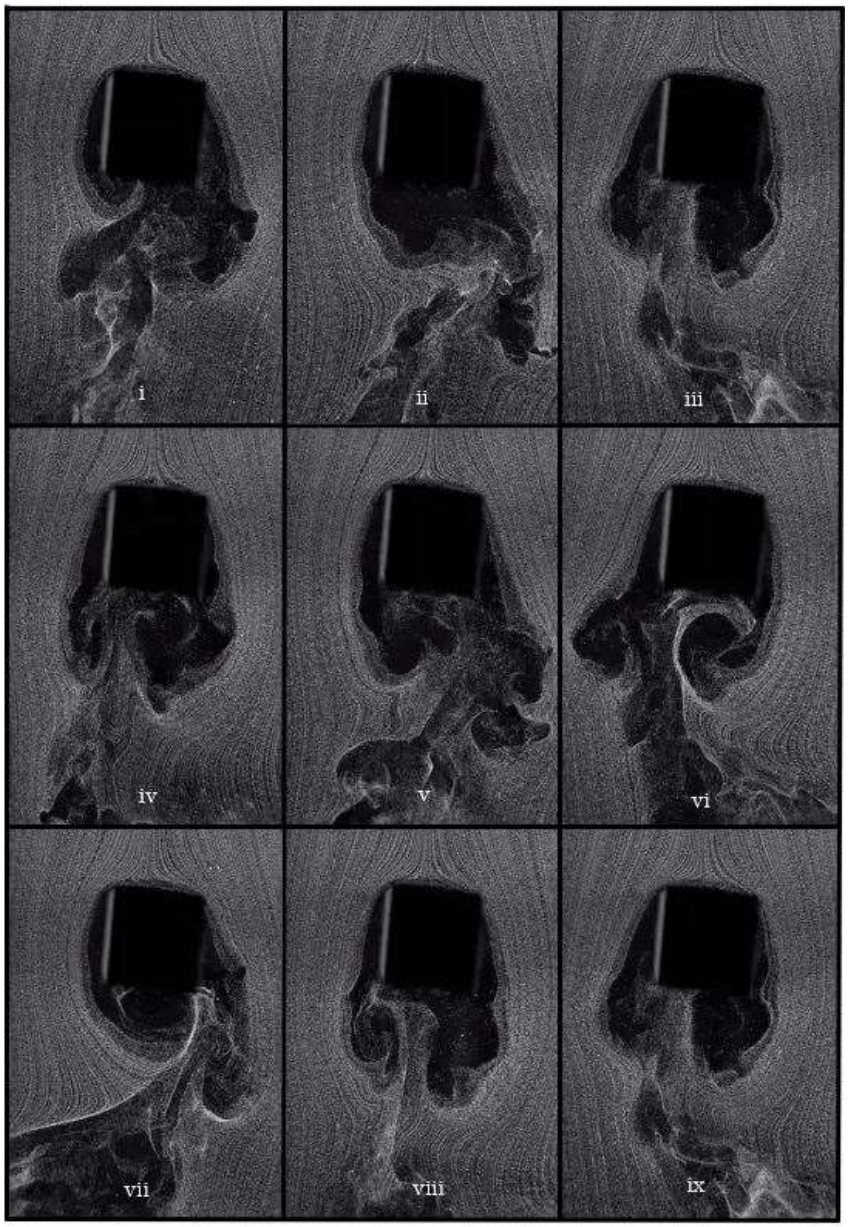

Figure 27: Rough and asymmetric shedding for $U^* = 4$, $\alpha = 5°$.

3.7 Remarks on the Transition to Asymmetry

It is an interesting finding that a small amount of passive asymmetry (for the same value of reduced velocity) excites a more alternating style of shedding from the square prism.

This transition can be seen in figure 28b, where the ratio of fluctuating coefficient of lift to coefficient of drag amplitude, R_f, is plotted as a function of U^*. Also evident from figure 28 is that for low values of α, where the structure is very near symmetric, this transition to asymmetry also exists with increasing U^*. This is similar to the type of transition that was seen for the circular cylinder in section 2.5 (see figure 5c) within the first region of response.

While it is tempting to conclude that this transition to asymmetry with increasing U^* is a phenomenon that occurs for all symmetric bluff bodies, a significant question remains unanswered. For $\alpha = 0°$, why does a displacement response with largely symmetric wake structures begin as late as $U^* = 3.2$, and correspond well with intersection of 2^*St and $f^* = 1$? In contrast, the circular cylinder begins its response much earlier ($U^* = 1.68$), and transitions from symmetry to asymmetry at values of U^* prior to any square prism response. It is possible that the range of Reynolds number has something to do with this discrepancy, but it has not been investigated in this study.

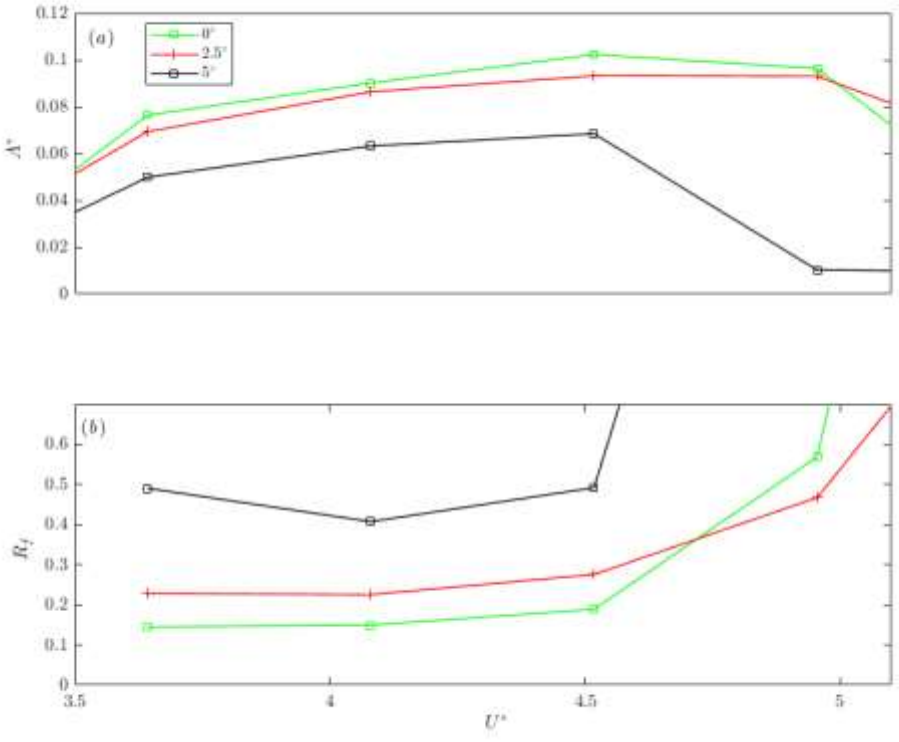

Figure 28: *(a)* Dimensionless displacement amplitude, A^*, and *(b)* the ratio of fluctuating lift to fluctuating drag, R_f, plotted against reduced velocity, U^*, within the region of the largest displacement amplitudes for $\alpha = 0°, 2.5°, 5°$.

3.8 High α Perturbed Wake Structures

The question of why sustained oscillations are not present at higher angles of incidence, α, is investigated briefly in this section by observing two cases of flow visualization at two angles of incidence, α = 20°, 30° at a reduced velocity U^* = 4. The flow visualization images are presented similarly to those presented in figures 25 and 27. For each case, the square prism system was given a small perturbation and the oscillations were allowed to decay.

Figure 30 shows the flow visualization for α = 20°. Upon being perturbed, two vortices of opposite sign on are formed on each side of the structure. Their initial positions seem to correlate well with the angle of the trailing face on their side. For example, in figure 30iii, the vortex on the left takes position farther downstream, as the trailing face on the left side of the prism projects father downstream than that on the right due to the angle of inclination α = 20°. This correlation is confirmed in figure 30iv. In this shot, the two vortices form in positions that correlate strongly with the angle of their respective trailing face. Only two vortex pairs are formed before the oscillations are damped out by the fluid.

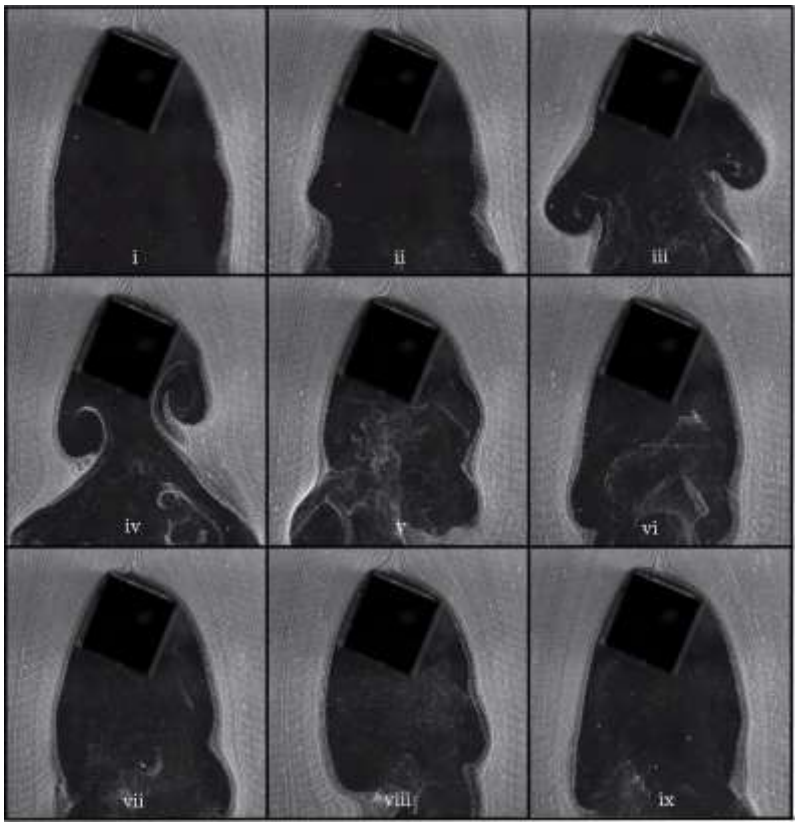

Figure 29: Vortex structures after a perturbation is given to the square prism at α = 20°

Flow visualization for α = 30° is shown in figure 31. A very similar pattern of shedding and decay is seen for this case. Two vortices of opposite sign are created by the structure upon perturbation. Their initial position correlates strongly with the angle of their respective trailing face, and the oscillations are damped out by the fluid after two vortex pairs are shed.

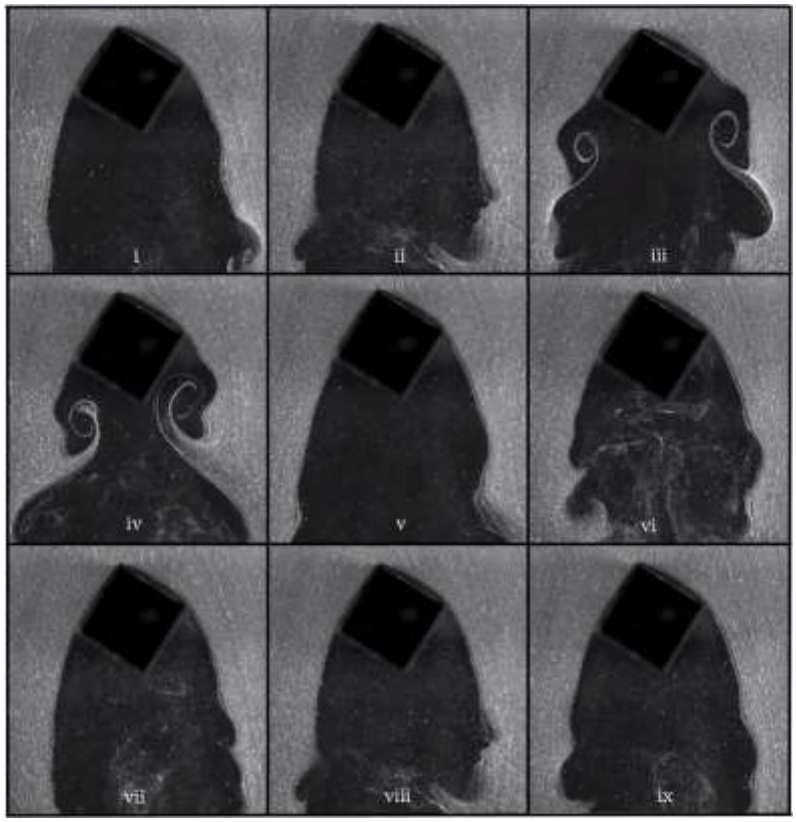

Figure 30: Vortex structures after a perturbation is given to the square prism at α = 30°

Based on these flow visualizations, the mechanism (or lack thereof) responsible for no sustained oscillations at higher angles of inclination can be discussed. When a vortex forms, it creates a region of low pressure near that part of the structure. It is this fluctuating pressure field that creates the time varying forces on a structure responsible for VIV (vortex induced vibrations). At high angles of inclination, it seems that the regions of low pressure near the inclined faces of the square prism may not project enough force in the direction of the degree of freedom to sustain oscillations. In the case of α = 0°, the rear face projects directly in the direction of the degree of freedom of the structure. As the passive asymmetry is introduced, the trailing faces project more and more in the direction of lift, and the pressure gradients across the

structure are felt less and less in the drag direction. Eventually, the magnitude of fluctuating drag forces is no longer enough to sustain oscillations, and the VIV is eliminated within this region of reduced velocity.

This argument is in no way a statement of fact, just thoughts based on the visualizations presented in figure 30 and 31. More work would be required (especially in investigating why a similar phenomenon does not occur for a flexibly mounted crossflow structure) to confirm or deny this theory.

CHAPTER 4
CONCLUDING REMARKS

The response of a circular cylinder allowed to exhibit pure translational motion in the streamwise direction to the incoming flow was studied experimentally over a range of reduced velocities of $1.4 < U^* < 4.4$, corresponding to a Reynolds number range of $970 < Re < 3370$. Displacement and force measurements, as well as flow visualizations, were conducted for every data point in the parameter range. It was found that the response of the pure translational inline system is consistent with previous studies on streamwise vibrations, (Aguirre 1977; Naudascher 1987; Okajima *et al*. 2002; Johansen 2004; Cagney & Balabani 2013a; Sherwood *et al*. 2009) in that two distinct regions of response are found, separated by a region of low-amplitude oscillations. The first region is generally characterized by symmetric vortex shedding, while the second one is characterized by asymmetric shedding, more typical of bluff body vortex shedding.

The symmetric shedding within the first region was found to transition gradually into asymmetry. This transition is captured in the form of a new wake mode, which is called Alternating-Symmetric (AS). This mode is characterized by two vortices of opposite signs, shedding simultaneously per cycle, but which alternate in size relative to one another. The transition to asymmetry was quantified in the reduced velocity range of $2.19 \leq U^* \leq 2.36$ using the ratio of the magnitude of fluctuating lift to fluctuating drag, R_f. In this region, the ratio is in the range of $0.115 < R_f < 0.169$, which indicates a larger magnitude of fluctuating lift than for $U^* < 2.19$. Additionally, within this region, the time history of fluctuating lift begins to show frequency content equal to $f_{nw}/2$. This frequency peak is only possible because the AS vortices alternate in size relative to one another, and do so for each cycle of oscillations.

As discussed in Section 3, oscillations in the majority of the first region are known to be excited by symmetric shedding. Previous studies (Naudascher 1987; Konstantinidis and Balabani 2007) have confirmed that symmetric shedding is a result of the in-line flow velocity fluctuations relative to the structure. In the present study, during the beginning of each test run, an initial perturbation was given to the structure at every reduced velocity. Once oscillations started, the structure was not perturbed for the rest of the test. It was found that the symmetric shedding does not manifest itself without an initial perturbation of the system, consistent with previous studies. Depending on experimental factors, the flow velocity at which symmetric shedding started would vary if the system were not perturbed. Even the smallest amount of structural vibration was shown to be capable of inducing this small relative fluctuation and

therefore symmetric shedding. In an inherently imperfect experimental environment, changes in air bearing pressure or water tunnel motor vibrations were capable of disturbing the structure enough to induce symmetric shedding which would quickly grow towards a limit cycle oscillation of the structure.

In the small-amplitude response region, a competition exists between the symmetric shedding, a product of streamwise circular cylinder oscillations, and the asymmetric shedding, a product of a bluff body in flow. The competition begins at lower U^* values of the first non-zero-amplitude response region, where ``perfectly symmetric'' vortices win the battle. This symmetric shedding pattern gives way to the Alternating Symmetric (AS) pattern as competition heats up between the two modes (symmetric and asymmetric). The competition ends approximately when the expected asymmetric shedding frequency based on the Strouhal Law becomes equal to one half the system's natural frequency, and the second region of non-zero-amplitude response begins.

The near wake modes and their corresponding U^* range are listed in table 2. This study is the first in which the gradual transition from symmetry to asymmetry has been described in the form of the AS shedding mode, seen briefly for $2.19 < U^* < 2.36$

Table 2: Wake modes as seen in this study.

Reduced Velocity	**Shedding Mode**
$1.68 \leq U^* \leq 2.1$	Symmetric
$2.19 \leq U^* \leq 2.36$	Alternate Symmetric
$2.4 \leq U^* \leq 2.85$	Competitive
$2.9 \leq U^* \leq 3.8$	Asymmetric

The response of a square prism allowed to exhibit pure translational motion in the streamwise direction to the incoming flow was also studied experimentally over a range of reduced velocities of $2.4 < U^* < 5.8$, corresponding to a Reynolds number range of $757 < Re < 1900$, at all angles of incidence shown in table 1. Displacement and force measurements were conducted at each point in the parameters space. The system was found to exhibit a non-zero amplitude response for angles of incidence, $\alpha = 0°, 2.5°, 5°, 7.5°$. The amplitude and reduced velocity range for which this response existed was found to decrease with increasing α. The frequency response of displacement and coefficient of lift were examined for each of these angles of incidence and it was found that the structure was locked in over the entire response range for $\alpha = 0°, 2.5°, 5°, 7.5°$.

For the symmetric case of $\alpha = 0°$, these oscillations were sustained by a rough form of symmetric shedding. As the angle of incidence was increased, this shedding progressed to a more asymmetric pattern, as evident by flow visualization at $\alpha = 5°$, and spectral contents of coefficients of lift and drag. It was also found that, for low values of α, there existed a gradual transition to a more asymmetric fluid forcing with increasing reduced velocity U^*.

Flow visualization was conducted for higher angles of incidence $\alpha = 20°, 30°$. Vortex structures that formed upon a perturbation of the structure were speculated to not project enough force in the direction of the degree of freedom to sustain oscillations.

In general, it seems that these flexibly mounted bluff bodies with a degree of freedom in the streamwise direction offer a glimpse into ordered, symmetric flow patterns. In both cases however, changing parameters create gradual bifurcations in which this symmetry breaks down, and makes way for the more typical asymmetric patterns typically associated with flow around a bluff body. In the case of the circular cylinder, the symmetric pattern is more ordered to begin with, and transitions gently to asymmetry with increasing U^*. The wake of the square prism is less laminar and transitions quickly to asymmetry with increasing angle of incidence, and also increasing U^* at the lowest angles of incidence.

BIBLIOGRAPHY

Aguirre, J.E., 1977. Flow Induced, In-line Vibrations of a Circular Cylinder. Ph.D. Thesis, Imperial College of Science and Technology.

Al-Mdallal, Q., Lawrence, K., & Kocabiyik, S. (2007). Forced streamwise oscillations of a circular cylinder: Locked-on modes and resulting fluid forces. Journal of Fluids and Structures, 23(5), 681-701. doi:10.1016/j.jfluidstructs.2006.11.001

Bearman, P. (1984). Vortex Shedding from Oscillating Bluff Bodies. Annual Review of Fluid Mechanics, *16*(1), 195-222. doi:10.1146/annurev.fluid.16.1.195

Bearman, P., Gartshore, I., Maull, D., & Parkinson, G. (1987). Experiments on flow-induced vibration of a square-section cylinder. Journal of Fluids and Structures,1(1), 19-34. doi:10.1016/s0889-9746(87)90158-7

Blevins, R. D. (1990). *Vortex Induced Vibrations*. Van Nostrand Reinhold.

Bourguet, R., & Jacono, D. L. (2015). In-line flow-induced vibrations of a rotating cylinder. Journal of Fluid Mechanics, 781, 127-165. doi:10.1017/jfm.2015.477

Cagney, N., & Balabani, S. (2013a). Wake modes of a cylinder undergoing free streamwise vortex-induced vibrations. Journal of Fluids and Structures, 38, 127-145. doi:10.1016/j.jfluidstructs.2012.12.004

Cagney, N., & Balabani, S. (2013b). Mode competition in streamwise-only vortex induced vibrations. Journal of Fluids and Structures, 41, 156-165. doi:10.1016/j.jfluidstructs.2013.02.009

Cagney, N., & Balabani, S. (2014). Streamwise vortex-induced vibrations of cylinders with one and two degrees of freedom. Journal of Fluid Mechanics, 758, 702-727. doi:10.1017/jfm.2014.521

Gopalkrishnan, R. (1993). Vortex-induced forces on oscillating bluff cylinders (Unpublished doctoral dissertation). Massachusetts Institute of Technology.

Dutta, S., Panigrahi, P. K., & Muralidhar, K. (2008). Experimental Investigation of Flow Past a Square Cylinder at an Angle of Incidence. Journal of Engineering Mechanics,134(9), 788-803. doi:10.1061/(asce)0733-9399(2008)134:9(788)

Jauvtis, N., & Williamson, C. H. (2004). The effect of two degrees of freedom on vortex-induced vibration at low mass and damping. Journal of Fluid Mechanics, 509, 23-62. doi:10.1017/s0022112004008778

Johansen, T., 2004. Hydrodynamic coefficients for vortex-induced vibrations in current direction. Master's thesis, Norwegian University of Science and Technology

King, R., 1977. A review of vortex shedding research and its application. Ocean Engineering 4, 141–171.

King, R., Prosser, M.J., Johns, D.J., 1973. On vortex excitation of model piles in water. Journal of Sound and Vibration 29,
169–188.

Knisely, C. (1990). Strouhal numbers of rectangular cylinders at incidence: A review and new data. Journal of Fluids and Structures,4(4), 371-393. doi:10.1016/0889-9746(90)90137-t

Konstantinidis, E. (2014). On the response and wake modes of a cylinder undergoing streamwise vortex-induced vibration. Journal of Fluids and Structures, 45, 256-262. doi:10.1016/j.jfluidstructs.2013.11.013

Konstantinidis, E., & Balabani, S. (2007). Symmetric vortex shedding in the near wake of a circular cylinder due to streamwise perturbations. Journal of Fluids and Structures, 23(7), 1047-1063. doi:10.1016/j.jfluidstructs.2007.03.002

Naudascher, E., 1987. Flow-induced streamwise vibrations of structures. Journal of Fluids and Structures 1, 265–298.

Naudascher, E. and Rockwell, D. (1994) Flow-Induced Vibrations: An Engineering Guide. Dover Publications, Inc., Mineola, New York.

Nishihara, T., Kaneko, S., Watanabe, T., 2005. Characteristics of fluid dynamic forces acting on a circular cylinder oscillated in the streamwise direction and its wake patterns. Journal of Fluids and Structures

Nemes, A., Zhao, J., Jacono, D. L., & Sheridan, J. (2012). The interaction between flow-induced vibration mechanisms of a square cylinder with varying angles of attack. *Journal of Fluid Mechanics,710*, 102-130. doi:10.1017/jfm.2012.353

Obasaju, E. (1983). An Investigation of the Effects of Incidence on the Flow Around a Square Section Cylinder. Aeronautical Quarterly,34(04), 243-259. doi:10.1017/s0001925900009768

Okajima, A., Kosugi, T., & Nakamura, A. (2002). Flow-Induced In-Line Oscillation of a Circular Cylinder in a Water Tunnel. Journal of Pressure Vessel Technology, 124(1), 89. doi:10.1115/1.1430670

Paidoussis, Michael & J. Price, Stuart & de Langre, Emmanuel. (2010). Fluid-structure Interactions: Cross-flow-induced Instabilities. Fluid-Structure Interactions: Cross-Flow-Induced Instabilities. 1-402. 10.1017/CBO9780511760792.

Rockwell, D. O. (1977). Organized Fluctuations Due to Flow Past a Square Cross Section Cylinder. Journal of Fluids Engineering,99(3), 511. doi:10.1115/1.3448831

Sarpkaya, T. (2003). A Critical Review of the Intrinsic Nature of Vortex Induced Vibrations. Journal of Fluids and Structures. doi:10.21236/ada417156

Seyed-Aghazadeh, B., Carlson, D. W., & Modarres-Sadeghi, Y. (2017). Vortex-induced vibration and galloping of prisms with triangular cross-sections. Journal of Fluid Mechanics, 817, 590-618. doi:10.1017/jfm.2017.119

Sherwood, J., Dusting, J., Konstantinidis, E., & Balabani, S. (2009). Flow-Induced Streamwise Vibration of a Flexibly-Mounted Cantilevered Cylinder in Steady and Pulsating Crossflow. Volume 4: Fluid-Structure Interaction. doi:10.1115/pvp2009-77293

Ulveseter, J., Sævik, S., & Larsen, C. (2017). Time domain model for calculation of pure in-line vortex-induced vibrations. Journal of Fluids and Structures, 68, 158-173. doi:10.1016/j.jfluidstructs.2016.10.013
Vandiver, J. K. (2012). Damping Parameters for flow-induced vibration. Journal of Fluids and Structures, 35, 105-119. doi:10.1016/j.jfluidstructs.2012.07.00

Williamson, C. H., & Govardhan, R. (2004). Vortex-Induced Vibrations. Annual Review Fluid Mechanics. doi:10.1146/annurev.fluid.36.050802.122128